(2)

Applied Research Laboratory

Technical Report

DEVELOPMENT AND USE OF AN X-RAY INDUCED FLUORESCENCE SYSTEM DESIGNED TO MEASURE REGIONAL MYOCARDIAL PERFUSION

by

Bradley M. Palmer

PENNSTATE

The Pennsylvania State University
APPLIED RESEARCH LABORATORY
P.O. Box 30
State College, PA 16804

DEVELOPMENT AND USE OF AN X-RAY INDUCED FLUORESCENCE SYSTEM DESIGNED TO MEASURE REGIONAL MYOCARDIAL PERFUSION

by

Bradley M. Palmer

Technical Report No. TR 91-010
October 1991

A-1

Supported by:
Space and Naval Warfare Systems Command

L.R. Hettche, Director
Applied Research Laboratory

Approved for public release; distribution unlimited

91 10 28 11

REPORT DOCUMENTATION PAGE

Form Approved
OMB No. 0704-0188

1. AGENCY USE ONLY (Leave blank)	2. REPORT DATE	3. REPORT TYPE AND DATES COVERED
	August 1989	

4. TITLE AND SUBTITLE
Development and use of an X-Ray Induced Fluorescence system designed to measure regional myocardial perfusion

5. FUNDING NUMBERS
N-00039-88-C-0051

6. AUTHOR(S)
Bradley M. Palmer

7. PERFORMING ORGANIZATION NAME(S) AND ADDRESS(ES)
Penn State University
Applied Research Laboratory
P.O. Box 30
State College, PA 16804

8. PERFORMING ORGANIZATION REPORT NUMBER
TR# 91-010

9. SPONSORING / MONITORING AGENCY NAME(S) AND ADDRESS(ES)
Space and Naval Warfare Systems Command
Department of the Navy
Washington, DC 20363-5100

10. SPONSORING / MONITORING AGENCY REPORT NUMBER

11. SUPPLEMENTARY NOTES

12a. DISTRIBUTION / AVAILABILITY STATEMENT

12b. DISTRIBUTION CODE

13. ABSTRACT *(Maximum 200 words)*

The need to measure regional myocardial perfusion noninvasively, both for clinical and for research purposes, has resulted in the development of several measurement techniques. In the present work, an attempt was made to produce a system for measuring regional myocardial perfusion based on X-ray induced fluorescence of an iodinated flow tracer. The system's development concentrated on the need to measure accurately the tracer concentration transients which would arise in an intact heart after a tracer's intravenous injection. The subsequent analysis of these transients was also developed here in order to provide a quantitative measure of bloom perfusion based on a mathematical model of tracer transport through the coronary vasculature.

An evaluation of the system's ability to produce accurate measurements of regional myocardial perfusion *in vivo* was also undertaken. In 13 open-chested canines, X-ray induced fluorescence was used to monitor the iodine concentration transients which arose in the left ventricular lumen and in a discrete region of the myocardium after an intravenous injection of iodinated flow tracer. Deconvolution of the recorded transients in the frequency domain produced a transfer function from which the mean transit time for the tracer to travel from the left ventricular lumen to the myocardium was calculated. Measurements of regional myocardial perfusion of radioactive microspheres were used as standards to which the reciprocals of the mean transit times were compared. Subsequent linear regression analysis produced a correlation coefficient of $r = 0.71$. Comparison of the relative change in perfusion with the relative change in the respective reciprocals of mean transit times produced a linear correlation coefficient of $r = 0.88$.

14. SUBJECT TERMS	15. NUMBER OF PAGES
X-Ray Induced Fluorescence, myocardial perfusion, non-invasively, iodinated flow tracer	119
	16. PRICE CODE

17. SECURITY CLASSIFICATION OF REPORT	18. SECURITY CLASSIFICATION OF THIS PAGE	19. SECURITY CLASSIFICATION OF ABSTRACT	20. LIMITATION OF ABSTRACT
Unclassified	Unclassified	Unclassified	

GENERAL INSTRUCTIONS FOR COMPLETING SF 298

The Report Documentation Page (RDP) is used in announcing and cataloging reports. It is important that this information be consistent with the rest of the report, particularly the cover and title page. Instructions for filling in each block of the form follow. It is important to ***stay within the lines*** to meet ***optical scanning requirements***.

Block 1. Agency Use Only *(Leave blank)*.

Block 2. Report Date. Full publication date including day, month, and year, if available (e.g. 1 Jan 88). Must cite at least the year.

Block 3. Type of Report and Dates Covered. State whether report is interim, final, etc. If applicable, enter inclusive report dates (e.g. 10 Jun 87 - 30 Jun 88).

Block 4. Title and Subtitle. A title is taken from the part of the report that provides the most meaningful and complete information. When a report is prepared in more than one volume, repeat the primary title, add volume number, and include subtitle for the specific volume. On classified documents enter the title classification in parentheses.

Block 5. Funding Numbers. To include contract and grant numbers; may include program element number(s), project number(s), task number(s), and work unit number(s). Use the following labels:

C	- Contract	PR	- Project
G	- Grant	TA	- Task
PE	- Program Element	WU	- Work Unit Accession No.

Block 6. Author(s). Name(s) of person(s) responsible for writing the report, performing the research, or credited with the content of the report. If editor or compiler, this should follow the name(s).

Block 7. Performing Organization Name(s) and Address(es). Self-explanatory.

Block 8. Performing Organization Report Number. Enter the unique alphanumeric report number(s) assigned by the organization performing the report.

Block 9. Sponsoring/Monitoring Agency Name(s) and Address(es). Self-explanatory.

Block 10. Sponsoring/Monitoring Agency Report Number. *(If known)*

Block 11. Supplementary Notes. Enter information not included elsewhere such as: Prepared in cooperation with..., Trans. of...; To be published in.... When a report is revised, include a statement whether the new report supersedes or supplements the older report.

Block 12a. Distribution/Availability Statement. Denotes public availability or limitations. Cite any availability to the public. Enter additional limitations or special markings in all capitals (e.g. NOFORN, REL, ITAR).

DOD	- See DoDD 5230.24, "Distribution Statements on Technical Documents."
DOE	- See authorities.
NASA	- See Handbook NHB 2200.2.
NTIS	- Leave blank.

Block 12b. Distribution Code.

DOD	- Leave blank.
DOE	- Enter DOE distribution categories from the Standard Distribution for Unclassified Scientific and Technical Reports.
NASA	- Leave blank.
NTIS	- Leave blank.

Block 13. Abstract. Include a brief *(Maximum 200 words)* factual summary of the most significant information contained in the report.

Block 14. Subject Terms. Keywords or phrases identifying major subjects in the report.

Block 15. Number of Pages. Enter the total number of pages.

Block 16. Price Code. Enter appropriate price code *(NTIS only)*.

Blocks 17. - 19. Security Classifications. Self-explanatory. Enter U.S. Security Classification in accordance with U.S. Security Regulations (i.e., UNCLASSIFIED). If form contains classified information, stamp classification on the top and bottom of the page.

Block 20. Limitation of Abstract. This block must be completed to assign a limitation to the abstract. Enter either UL (unlimited) or SAR (same as report). An entry in this block is necessary if the abstract is to be limited. If blank, the abstract is assumed to be unlimited.

ABSTRACT

The need to measure regional myocardial perfusion noninvasively, both for clinical and for research purposes, has resulted in the development of several measurement techniques. In the present work, an attempt was made to produce a system for measuring regional myocardial perfusion based on X-ray induced fluorescence of an iodinated flow tracer. The system's development concentrated on the need to measure accurately the tracer concentration transients which would arise in an intact heart after a tracer's intravenous injection. The subsequent analysis of these transients was also developed here in order to provide a quantitative measure of blood perfusion based on a mathematical model of tracer transport through the coronary vasculature.

An evaluation of the system's ability to produce accurate measurements of regional myocardial perfusion *in vivo* was also undertaken. In 13 open-chested canines, X-ray induced fluorescence was used to monitor the iodine concentration transients which arose in the left ventricular lumen and in a discrete region of the myocardium after an intravenous injection of iodinated flow tracer. Deconvolution of the recorded transients in the frequency domain produced a transfer function from which the mean transit time for the tracer to travel from the left ventricular lumen to the myocadium was calculated. Measurements of regional myocardial perfusion by radioactive microspheres were used as standards to which the reciprocals of the mean transit times were compared. Subsequent linear regression analysis produced a correlation coefficient of r = 0.71. Comparison of the relative change in perfusion with the

relative change in the respective reciprocals of mean transit times produced a linear correlation coefficent of r = 0.88.

Based on the results of these studies, it was concluded that X-ray induced fluorescence provides accurate, external monitoring of iodine transients in very small regions of the myocardium *in vivo*. The reciprocal of the mean transit time was found to be an unacceptable estimator of absolute perfusion; however, accurate measurements of relative changes in regional myocardial perfusion were possible. Further study is recommended in modifying the tracer transport model to facilitate prediction of absolute flows and in evaluating the system's effectiveness with closed-chested subjects.

TABLE OF CONTENTS

LIST OF FIGURES

LIST OF TABLES

Chapter 1

INTRODUCTION

Ischemic heart disease refers to the inability of the coronary vasculature to supply the myocardium with a blood flow that is sufficient for the delivery of chemical substrates and the clearance of metabolic wastes necessary to maintain a specific demand for cardiac output. A reduction in the lumenal cross-sectional area of any portion of one or more coronary arteries as a result of atherosclerosis is the foremost cause of ischemic heart disease. Coronary atherosclerosis is almost exclusively responsible for episodes of angina pectoris, a result of transient myocardial ischemia which is often overcome by simply decreasing the demand for cardiac output through drug intervention or physical inactivity, as well as for prolonged myocardial ischemia which accounts for the nearly 1,000,000 survived myocardial infarctions and 600,000 deaths due to myocardial infarction or cardiogenic shock in the United States per year [Braunwald 1976; Silber 1987, p. 1017].

Due to these impressive statistics, ischemic heart disease due to coronary atherosclerosis has been recognized as the largest single cause of death in the Western World. It is therefore not surprising that the assessment of ischemic heart disease has become a virtual necessity in both clinical and research environments. For a clinician, a knowledge of myocardial perfusion, coronary flow reserve, i.e. the relative increase in coronary blood flow from rest which is available upon demand, and their spatial distributions is required to evaluate and localize areas under ischemic risk or the extent of myocardial damage

already sustained from an infarction. For research purposes, the measurement of regional myocardial perfusion is important for studying the effects of reduced blood supply on biochemical, electrical and mechanical properties of the myocardium, as well as for studying the physiologic compensatory mechanisms responsible for the protection of the myocardium during a blood flow deficit.

To meet the demands of the medical community, various techniques for measuring regional myocardial perfusion have been developed. All of these techniques are similar in that they require the introduction of a flow tracer into the coronary vasculature. In addition, these techniques are similar in their attempt to best meet the criteria of an "optimal" perfusion measuring device. These criteria can be represented by three main categories: accurate determination of perfusion, minimal invasiveness, and cost effectiveness.

The accuracy with which a device can measure perfusion is constrained by the ability of the specific technique to externally monitor a tracer and effectively interpret the data based on a realistic model of tracer kinetics. An optimal device would therefore be able to measure tracer concentration and distribution with both a high signal-to-noise ratio and good spatial resolution. This device would also be able to quantitate perfusion from the acquired data based on a valid model of tracer transport. The most successful models presently used describe tracer dynamics (indicator-dilution methods) or mechanisms of tracer uptake, where total tissue accumulation of the tracer reflects blood supply.

Restricting the invasiveness of a device has been the primary factor responsible for the seemingly slow development of an optimal technique. Invasive procedures can provide very accurate measurements of perfusion; however, these procedures are unacceptable for routine evaluation of myocardial perfusion in patients as well as for some animal research studies. An externally monitorable tracer is the key to meeting the noninvasive criterion. However, the tracer must not be toxic, and the procedure must neither put the subject at risk nor perturb the system under investigation.

One further restriction to be placed on the development of perfusion measurement devices is cost. The optimal device must be able to provide noninvasive, accurate measurements of myocardial perfusion at a cost which is acceptable to the patient, insurance company, or scientist, whoever is expected to pay for its use. And, as one might expect, the techniques currently available for measuring regional myocardial perfusion fall short of meeting at least one of the above optimal criteria.

Techniques for Measuring Myocardial Perfusion

Because atherosclerotic coronary artery disease is chiefly responsible for ischemic heart disease and does ultimately manifest itself as this physiologic disorder, the assessment of coronary artery disease can be used as a qualitative evaluation of ischemic risk [Silber 1987, p. 1012]. Conventional coronary angiography and the closely related digital subtraction angiography are currently the most often used techniques for visualizing and evaluating

coronary artery disease. These valuable techniques, however, require left heart catheterization, do not provide quantitative measurement of blood flow, and impart relatively high radiation doses to the patient and clinician. The attempt to quantify blood flow with these techniques has been termed digital densitography and involves conventional indicator-dilution analysis of contrast transients digitally produced from angiography films. Although digital densitography has been shown to provide some quantification of relative regional perfusion [Whiting et al. 1986] and bypass graft patency [Rutishauser et al. 1970], it does not relieve the associated invasiveness of the technique, i.e. catheterization and radiation dose.

Cinemagraphic Computed Tomography (Cine-CT), another technique employing densitography methods, has been recently introduced promising quantitative analysis of contrast transients without the need for catheterization [Lipton 1985]. With this ultrafast computed tomography technique, the contrast medium's concentration transients in the myocardium can be recorded with good signal-to-noise ratios and with reasonable spatial resolution [Boyd et al. 1979]. Preliminary studies using this technique show that the calculated index of perfusion, called CT-flow, has a strong linear correlation to flow measured by radioactive microspheres, a recognized standard for perfusion studies [Rumberger et al. 1987; Wolfkiel et al. 1987]. However, the technique has not yet produced actual values of tissue perfusion in units of blood flow per gram of tissue. This fact, the associated intense radiation [Brasch et al. 1978], and its relatively high cost [Lipton 1985] have limited the widespread acceptance of this technique for clinical work.

Currently, thallium-201 scanning is a very popular clinical tool used for measuring perfusion and coronary flow reserve requiring no catheterization [Strauss & Boucher 1986]. This technique, like other radionuclide techniques, relies on the tracer uptake by tissue, intracellular uptake in this case by way of the sodium-potassium adenosine triphosphate system [Strauss & Boucher 1986, p. 577], as a measure of its blood supply. The relatively noninvasive administration of this tracer allows for the evaluation of ischemia during exercise when myocardial blood flow is in demand. Although this technique does provide good qualitative measurements of relative myocardial perfusion, radiation delivery to non-target organs limits the signal intensity required for quantitative determination of blood flow to discrete regions of the myocardium [Tamaki et al. 1982].

Probably the most thought provoking technique to be recently developed is Positron Emission Tomography (PET). PET requires the intravenous injection or inhalation of a positron emitting tracer (such as carbon-11, nitrogen-13, oxygen-15, or rubidium-82) and, like the other radionuclide techniques, relies on tracer uptake to reflect blood supply [Bergmann et al. 1985]. During a presentation given by Bergmann et al. [1988], PET was reported to be able to provide measurements of myocardial perfusion in a discrete region of 5 cm x 4 cm x 4 cm while correlating very well ($r = 0.96$) with perfusion measured by radioactive microspheres. Because most positron emitting tracers decay with very little radiation dose imparted to the subject, the only, yet overwhelming disadvantage associated with the use of this technique is economic. The extraordinary cost of production, maintenance and

operation has allowed only a few institutions in this country to afford PET, and the prospects for its widespread availability within the foreseeable future is not good [Mullani & Gould 1984].

There is certainly more that can be said about the techniques described above. A more thorough review of these and other techniques has been given recently by Marcus et al. [1987]. Their review ends by stating a few goals for future techniques under development. These goals can be paraphrased as the following: 1) to determine actual or relative myocardial perfusion quantitatively, 2) to be able to assess perfusion in different transmural layers of the left ventricle therefore requiring very good spatial resolution, 3) to provide measurements without catheterization nor excessive radiation, and 4) to do all this at a reasonable cost. The developing techniques mentioned by Marcus et al. [1987] are presently unable to meet all of these goals, particularly the measurement of perfusion with the spatial resolution required for transmural differentiation. Therefore, a technique which could successfully measure absolute or relative regional myocardial perfusion while meeting the spatial resolution requirement would be of considerable value.

It has been suggested that a technique based on the X-ray induced fluorescence of iodine be developed for the purpose of measuring myocardial perfusion in very discrete regions of the myocardium [McInerney et al. 1987]. The system would monitor the rate of characteristic X-ray emission from iodine as it passed through regions of the heart and would then relate the properties of the tracer's kinetics to blood flow. In an attempt to meet the four

goals outlined above, the X-ray induced fluorescence system would have to be able to perform the following: 1) accurately monitor tracer concentration transients in very discrete regions (no larger than 1 cm x 1 cm x 1 cm) of the myocardium after an intravenous injection of the flow tracer, 2) quantitate perfusion in absolute or relative terms based on these tracer transients, 3) impart a reasonably acceptable radiation dose to the subject being investigated, and 4) be cost effective.

In order to meet the four goals outlined above, the specific system suggested would be designed to monitor iodine concentration transients which arise in the left ventricular lumen and in a discrete region of the myocardium after an intravenous injection of an iodinated flow tracer. In order to calculate perfusion, the system would require an indicator-dilution model of tracer transport through the coronary vasculature such that recorded tracer transients could be analyzed to produce a measure of absolute or relative perfusion. Invasiveness would be handled favorably by requiring the intravenous injection and by restricting the radiation dose to an acceptable level and the local region of interest. In addition, the criterion of cost effectiveness would be met quite easily if the technique proved to be effective, principally because producing an X-ray fluorescence system is relatively inexpensive as compared to the cost of comparable devices like Cine-CT.

Purpose of This Dissertation

The purpose of this dissertation is to describe the development of a prototype X-ray induced fluorescence system which measures regional myocardial perfusion *in vivo* and to assess the efficacy of this technique based on perfusion studies performed with a canine model.

The process of fluorescence and the accuracy with which the concentration of an iodinated flow tracer can be monitored using this technique were important considerations and are discussed in Chapter 2. Chapter 3 is devoted to describing the X-ray fluorescence system developed during the course of this work. Specific details about hardware, spatial resolution, data acquisition, optimization, and performance are presented.

A model of tracer transport through the coronary vasculature was also required so that an analysis of the tracer transients would produce a measure of perfusion. A theoretical model of tracer transport is presented in Chapter 4. Based on the results of the model, the mean time required for a tracer to travel from the left ventricular lumen to the region of interest in the myocardium was found to be related to blood flow. The reciprocal of this mean transit time was then chosen as an index of perfusion. The transfer function analysis procedure used to determine the mean transit time from the tracer concentration transients is also described in Chapter 4.

In order to demonstrate the use and effectiveness of the X-ray fluorescence system, myocardial perfusion studies have been performed in a canine model using this technique. The aim of these studies was to compare perfusion measured by the fluorescence system with that measured by radioactive microspheres. A description of these validation studies and their results are given in Chapter 5. The analysis of data acquired from a series of dogs included not only a comparison of the perfusion measured by the microspheres with the reciprocal of the mean transit time, but also the comparison of relative changes in perfusion measured by the microspheres with relative changes found using the fluorescence system. These latter results should demonstrate the technique's usefulness in measuring coronary flow reserve.

The effectiveness of this technique in providing a measure of absolute or relative perfusion in very discrete regions of the myocardium should be evident from these experiments. This thesis will conclude by assessing the possible usefulness of the X-ray fluorescence system in determining perfusion in close-chested animals, and in humans, based on the results of these studies.

Chapter 2

USE OF X-RAY INDUCED FLUORESCENCE

Any system used to measure the concentration of some element in a sample and which is based on the process of X-ray induced fluorescence must be able to induce the element to fluorescence, detect the fluorescence photons emitted from the sample, and then discern the element's concentration. For the purpose of monitoring the concentration of a tracer within an intact biological system, it is important to choose a tracer which is not only innocuous to that system, but will also fluoresce with an efficiency and energy that will allow for accurate external monitoring. These criteria are presently best met by iodine.

Iodine is nontoxic to biological systems even at relatively high concentrations and possesses favorable fluorescence characteristics, the details of which will be presented later in this chapter. Another important advantage of iodine is its acceptability by the medical community. Iodine is the integral constituent of radiographic contrast agents which are currently used as tracers in various modes of angiography. Therefore, iodine's use in biological systems is well understood and accepted.

At the onset of the work reported here, questions quickly arose concerning the relationship between fluorescence and iodine concentration and the accuracy with which iodine concentration can be ascertained. Therefore, before making any measurements of iodine concentration using

the X-ray fluorescence system, let alone perfusion, it was considered necessary to study the nature of X-ray fluorescence and its use.

The remainder of this chapter deals solely with material which is pertinent to the understanding of the fluorescence process, its use in determining iodine concentrations and the accuracy with which estimates of iodine concentration can be made. The physical process of fluorescence photon emission is first presented where the relationship between iodine concentration and fluorescence is derived. The photon interactions which influence the detection of background radiation are also described. The final relationships of fluorescence and background radiation to iodine concentration are then given.

This chapter also presents an existing model of the statistical nature by which photon detection is governed. This model is employed to determine the accuracy with which iodine concentration measurements are made with X-ray induced fluorescence. The influence of system characteristics on accuracy is expressed quantitatively through this model, thereby facilitating a stategy for system optimization. The importance of having derived the relationships between fluorescence, background radiation and iodine concentration will become quite evident when considering the specific modifications of an X-ray fluorescence system which produce the most accurate measurements of iodine concentration.

The Fluorescence Process

X-ray induced fluorescence is an atomic level process which is initiated by an externally produced X-ray photon colliding with an atom's electron field. If the photon is of sufficient energy, an electron may be ejected from the atom (the photoelectric effect) leaving an orbital vacancy. In order for the atom to reestablish its ground state, an electron from a higher orbit will fill this vacancy and, in doing so, will release energy in the form of an X-ray photon. This photon emission is termed fluorescence.

Only very specific electron orbital transitions can occur; the various schemes of allowable transitions in multi-electron atoms are presented well by Russ [1984, pp. 1-9]. The energy of a fluorescence photon which arises from any one transition is equal to the difference in the binding energies of the original and destination electron orbits involved. Because binding energies of electrons are dependent upon the atomic number of the atom, the energy difference associated with the various transitions are characteristic of the element. Due to this fact, fluorescence has been used quite extensively for identifying elements and for determining their concentrations in samples of unknown constituents.

Deciding which fluorescence photons were to be used for determining iodine concentrations *in vivo* was not a difficult task. If the sample to be analyzed for iodine content were deep in a thorax, as the heart is, then it would be necessary to induce fluorescence with X-rays that can penetrate the thorax.

It would also be necessary to observe fluorescence photons of sufficient energy that they could escape from a closed thorax. The only orbital transitions in iodine which meet these criteria occur from K-shell vacancies induced by X-ray photons of at least 33.2 keV, the energy known as the K-edge for iodine. The transitions which then produce fluorescence are the L-shell to K-shell transitions, which emit so-called K_α photons of 28.3 and 28.6 keV, and the M-shell to K-shell transitions, which produce K_β photons of about 32.2 and 32.3 keV [CRC Press 1974, p. 11].

Figure 2.1 shows an energy spectrum of photons detected from an irradiated sample known to contain iodine. The fluorescence photons of iodine are indicated in the figure as is the spectrum of scattered X-rays of the irradiating beam. From the figure, it is clear that K_α photons are emitted much more often than K_β photons. It is also clear that if the energy of the K_α photons is monitored, then background radiation which cannot be attributed to fluorescence will also be observed. Therefore, because K_α photon detection rate is used to deduce iodine content, it was necessary to determine the relationship between K_α photon detection rate, background X-ray detection and iodine concentration.

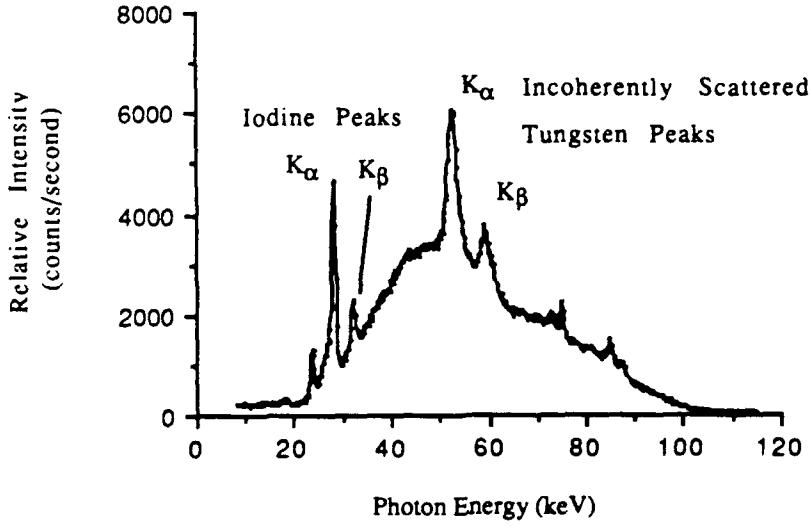

Figure 2.1: Typical Energy Spectrum Detected from an Irradiated Sample. The fluorescence peaks of the iodine are prominent, as are the fluorescence peaks of lead and indium from the detector's collimator and the incoherently scattered tungsten fluorescence peaks emitted from the X-ray generator's anode. The broad, background spectrum represents the photons which are scattered from the sample into the photon detector.

Fluorescence Related to Iodine Concentration

Finding the relationship between K_α photon detection and iodine concentration requires following a long tortuous path of describing the many interaction between X-rays and matter. However, if this path is followed methodically, each step can be quite straightforward. The intermediate events which must be examined are the rate of production of K-shell vacancies, the rate of K_α photon emission, and then finally the rate of K_α photon detection.

Production of K-shell Vacancies

Producing K-shell vacancies requires the absorption of X-ray photons by K-shell electrons, one of many attenuation processes. In fact, the rate of K-shell vacancy production is equal to the fraction of the total attenuation which can be attributed to iodine's K-shell photoelectric effect. However, before presenting the model of vacancy production, it is important to understand first the attenuation processes involved.

A linear attenuation coefficient for a medium can be defined as the probability per unit pathlength that a photon will interact with the medium. In mathematical terms, the linear attenuation coefficient is used in the following differential equation which describes the decrease in a narrow beam's intensity over a distance dx within a medium [Hubbell 1969, p. 5]:

$$\frac{-dI(E,x)}{dx} = \mu(E)\, I(E,x) \qquad (2.1)$$

where I(E,x) = the intensity of the beam at energy E and at a point x and is given in units of #photons/sec-keV, and $\mu(E)$ = the linear attenuation coefficient which is also a function of energy and has units of reciprocal length, usually cm^{-1}. It should be noted that equation 2.1 is valid only when secondary scattering of photons back into the primary beam is negligible. The solution to equation 2.1 is given as:

$$I(E,x) = I(E,0)\, e^{-\mu(E)x} \tag{2.2}$$

where I(E,0) = the beam intensity at the boundary of the attenuating medium.

Because the constituents of different materials are never exactly alike, the intrinsic attenuation characteristics of any material are best represented by the mass attenuation coefficients of its constituents. The mass attenuation coefficient, call it $\mu'(E)$, is given in units of cm^2/g. Therefore, the total linear attenuation coefficient, call it $\mu_T(E)$, is then represented as the sum of the products of the mass attenuation coefficients and the concentrations for all elements present in the material:

$$\mu_T(E) = \sum_{j}^{all} \mu'_j(E)\rho_j \tag{2.3}$$

where $\mu_T(E)$ = the total linear attenuation coefficient in units of cm^{-1}, $\mu'_j(E)$ = mass attenuation coefficient of the j^{th} element in units of cm^2/g, and ρ_j = concentration of j^{th} element in g/cm^3.

Each element's mass attenuation coefficient represents the various interactions responsible for attenuation, like X-ray scattering and the photoelectric effect. Scattering of photons is described as either coherent (Rayleigh) or incoherent (Compton) scattering. The photoelectric effects of importance here involve K- and L-shell electrons. The total linear attenuation coefficient of equation 2.3 can therefore be rewritten as:

$$\mu_T(E) = \sum_{j}^{all} [\mu'_{jcoh}(E) + \mu'_{jincoh}(E) + \mu'_{jKpe}(E) + \mu'_{jLpe}(E)]\, \rho_j \qquad (2.4)$$

where the subscripts "coh," "incoh," and "pe" refer to attenuation by coherent scattering, incoherent scattering, and the photoelectric effect, respectively.

From equation 2.4, the fraction of the total attenuation which can be attributed to iodine K-shell photoelectric effect is simply $\mu'_{IKpe}(E)\rho_I / \mu_T(E)$. As stated earlier, the rate of K-shell vacancy production is equal to this fraction of the beam's attenuation. Therefore, for an X-ray beam travelling in the positive x-direction with an energy spectrum of I(E,x), the total number of K-shell vacancies produced per unit time, call it $K_v(x)$, which occurs in a volume of infinitesimal size dxdydz is given as:

$$d^3K_v(x) = \int_E \frac{\mu'_{IKpe}(E)\rho_I}{\mu_T(E)} \left[\frac{-dI(E,x)}{dx}\right] dE\, dxdydz \qquad (2.5)$$

It would be helpful if the rate of the decrease in beam intensity, used in equation 2.5, could be interpreted in analytical terms. With the use of the

equations 2.1 and 2.2, the rate of decrease in beam intensity can be expressed analytically as:

$$\frac{-dI(E,x)}{dx} = \mu_T(E)I(E,0)\ e^{-\mu T(E)x} \qquad (2.6)$$

and substituted into equation 2.5 to give:

$$d^3K_v(x) = \int_E \mu'_{IKpe}(E)\ \rho_I\ I(E,0)\ e^{-\mu T(E)x}\ dE\ dxdydz \qquad (2.7)$$

Equation 2.7 is now the analytical expression which represents the rate of iodine K-shell vacancy production at a linear distance x within a medium.

Rate of K-shell Fluorescence Emission

From the reoccupation of every K-shell vacancy there will be a fluorescence photon produced. It is possible, however, that this fluorescence photon will collide with the electron field of the parent atom. This collision may initiate the ejection of another electron, called an Auger (French pronunciation ~ "O-djay") electron. Therefore, the fraction of fluorescence photons which are actually emitted from the atom is termed the fluorescence yield. The fluorescence yield from K-shell vacancies, written ω_K, is dependent upon the atomic number and has a value for iodine of $\omega_{IK} = 0.882$ [Vaño & González 1978, p. 400; CRC Press 1974, p. 222].

The fraction of all emitted fluorescence photons which are K_α photons is termed the relative emission intensity of K_α, written $g_{K\alpha}$, and has a value for iodine of $g_{IK\alpha} = 0.82$ [Bertin 1975, p. 456]. Therefore, the rate of K_α photon emission from the volume dxdydz irradiated by a beam of intensity I(E,0), written here as $K_{\alpha e}(x)$, is equal to the rate of K-shell vacancy production multiplied by the fluorescence yield and the K_α relative emission intensity:

$$d^3K_{\alpha e}(x) = \omega_{IK}\, g_{IK\alpha}\, d^3K_v(x)$$

$$= \omega_{IK}\, g_{IK\alpha} \int_E \mu'_{IKpe}(E)\, \rho_I\, I(E,0)\, e^{-\mu T(E)x}\, dE\, dxdydz \qquad (2.8)$$

Rate of K_α Photon Detection

In practice, the photon detector is collimated to monitor only a small region irradiated by the beam. This small region is a finite volume which is bounded by the X-ray beam and the field of view of the collimated detector. If the incident beam is assumed to have a rectangular cross-section with sides of length Y and Z, and the field of view of a detector is assumed to be perfectly collimated to enclose a length X along the beam, then the integration over this volume will equal the total rate of K_α fluorescence emitted from this, the detector's so-called sensitive volume.

In order to determine the rate at which K_α photons are detected, consideration must also be given to the geometric relationship between the

beam and the detector. If the detector is positioned such that it observes only those photons which are emitted into the positive z-direction, then, because photons are emitted isotropically, only a fraction of emissions will travel in the z-direction toward the detector. This fraction is equal to the solid angle subtended by the detector, Ω_d, divided by 4π steradians. Consideration must also be given to the fact that K_α photons furthest from the detector will be attenuated as they travel through the sensitive volume. Therefore, the rate of K_α detection, call it $K_{\alpha d}$, is given as the integral over the sensitive volume with the factors of solid angle fraction and photon attenuation included in the expression:

$$K_{\alpha d} = \frac{\Omega_d}{4\pi} \omega_{IK}\, g_{IK\alpha}\, \rho_I \int_{XYZ}\int_{E} \mu'_{IKpe}(E)\, I(E,0)\, e^{-\mu_T(E)x}\, e^{-\mu_T(28.5)(Z-z)}\, dE\, dx dy dz \tag{2.9}$$

The exponential term $\exp[\, -\mu_T(28.5)(Z-z)\,]$ represents the effect of attenuation on fluorescence photons as they pass through the sensitive volume on their way toward the detector. It should be noted that the attenuation of incoming or outgoing photons due to material which is not part of the sensitive volume is ignored here.

If the spatial integrations of equation 2.9 are carried out, the detection rate of K_α photons from the detector's sensitive volume is found as:

$$K_{\alpha d} = \frac{\Omega_d}{4\pi} \omega_{IK}\, g_{IK\alpha}\, \rho_I\, Y \int_{E} \mu'_{IKpe}(E)\, I(E,0)\, \frac{[1-e^{-\mu_T(E)X}]}{\mu_T(E)}\, \frac{[1-e^{-\mu_T(28.5)Z}]}{\mu_T(28.5)}\, dE \tag{2.10}$$

Considering that the total linear attenuation coefficient, $\mu_T(E)$, is somewhat dependent upon iodine concentration, it would seem as though this relationship between K_α detection and iodine concentration, as given by equation 2.10, is quite complicated. However, if the total attenuation through the sensitive volume itself is quite small, despite iodine concentration, then the exponential terms of equation 2.7 can be approximated as linear terms. From the series expansion of the exponential, $e^{-x} = 1 - x + x^2/2 - x^3/3! + \cdots$, only the first two terms are significant when $x \leq 0.27$, a stipulation which ensures that higher order terms contribute less than 5% of the total value of the exponential. Therefore, the specific criteria which would allow for a linear approximation of the exponential terms in equation 2.10 are $\mu_T(E)X \leq 0.27$ and $\mu_T(28.5)Z \leq 0.27$. In order to test for these conditions, the subject of the total linear attenuation coefficient must be revisited.

The total linear attenuation coefficient, $\mu_T(E)$, is equal to the sum of the linear attenuation coefficients associated with each element in the volume. Because the only elements which will be found in the sensitive volume will be those associated with muscle, blood and the tracer, whose many constituents are similar, then the only two materials which will be considered here are iodine (I) and muscle (M). The total linear attenuation of the sensitive volume is then:

$$\mu_T(E) = [\mu'_{Iscat}(E) + \mu'_{Ipe}(E)]\,\rho_I + [\mu'_{Mscat}(E) + \mu'_{Mpe}(E)]\,\rho_M \qquad (2.11)$$

where the subscript "scat" refers to attenuation by all scattering processes.

To test the first stipulation, $\mu_T(E)X \leq 0.27$, consider the highest value of $\mu_T(E)$ which occurs at E = 33.2 keV, just above iodine's K-edge. Using values reported by Hubbell [1969], the value for the total linear attenuation coefficient defined in equation 2.11 becomes:

$$\mu_T(33.2) = [0.740 + 35.64]\,\rho_I + [0.229 + 0.144]\,\rho_M \qquad (2.12)$$

The maximum iodine concentration which can be expected is about 10 mg/ml, and the muscle concentration remains relatively constant at ~1.06 g/cm^3. Therefore, the value for the total linear attenuation coefficient is given as:

$$\mu_T(33.2) = 36.38\ (0.01) + 0.373\ (1.06) = 0.759\ cm^{-1} \qquad (2.13)$$

Based on this result, the stipulation $\mu_T(33.2)X \leq 0.27$ is met when $X \leq 0.36$ cm.

The condition $\mu_T(28.5)Z \leq 0.27$ can be tested in a similar manner. The total linear attenuation coefficient at 28.5 keV is found to have a value of $\mu_T(28.5) = 0.395\ cm^{-1}$, which requires $Z \leq 0.68$ cm. Therefore, the use of the linear approximation for the exponential terms in equation 2.10 is valid when $X \leq 0.36$ cm and $Z \leq 0.68$ cm. When these conditions are met, the fluorescence detection rate of equation 2.10 is found to be linearly proportional to the iodine concentration and can is written as follows:

$$K_{\alpha d} = \frac{\Omega_d}{4\pi}\,\omega_{IK}\,g_{IK\alpha}\,\rho_I\,XYZ \int_E \mu'_{IKpe}(E)\,I(E,0)\,dE \qquad (2.14)$$

As can be seen from equation 2.14, the proportionality constant which relates K_α photon detection to iodine concentration is dependent upon many factors, most notably the size of the sensitive volume, the fraction of solid angle field subtended by the detector, and the spectrum and intensity of the irradiating X-ray beam. Modifications of these factors will prove to be important for improving the performance of the X-ray fluorescence system.

Background Radiation

Background radiation refers to those X-ray photons which are detected by the photon detector in the same energy range as iodine's K_α photons, but which are not fluorescence photons. These photons are the product of incident X-rays scattering from the sensitive volume into the detector. Nearly all of the scattered X-rays which are detected at 28.5 keV are due to coherent (Rayleigh) or incoherent (Compton) scattering.

Incoherent scattering is an elastic collision between a photon and an electron whose binding energy to an atom is negligible compared to the energy of the photon. This process occurs most often in collisions involving the outer most electrons of molecules and atoms of low atomic number. The outcome of these collisions, like all other elastic collisions, is the scattering of both particles with final energies and directions which are in accordance with the conservation of energy and momentum. The energy of the scattered photon is therefore less than its incident energy by an amount dependent upon the angle at which it is deflected [Hubbell 1969, p. 27]. For photons which

have been scattered 90° into the detector, the original pre-scatter energy, E_O, is related to the detected post-scatter energy, E, by:

$$E_O = \frac{E}{(1 - E/511)} \quad keV \tag{2.15}$$

Therefore, background radiation detected at approximately 28.5 keV will be partly due to the incoherent scattering of X-rays which were originally of an energy $E_O \approx 30.2$ keV.

Coherent scattering refers to the process by which photons interact coherently with the electron orbits of an atom and then seem to be simply redirected without a change in energy. This process is one which occurs predominantly with atoms of high atomic numbers. Although biological tissue is composed primarily of elements of low atomic numbers, iodine has a relatively high atomic number. Therefore, coherent scattering from iodine is also considered in the following determination of the relationship between the rate of scatter detection and iodine concentration.

Relationship between Scatter and Iodine Concentration

The rate at which scattered photons reach the detector can be derived in much the same manner in which the K_α photon detection rate was derived. The rate of detected scatter is proportional to the fraction of the total attenuation which can be attributed to scatter processes, as well as the fraction of photons which are ultimately diverted toward the detector. It should be

noted, however, that the angular distribution of scattered photons is not isotropic and must be considered more thoroughly than in the fluorescence case.

The fraction of the total attenuation attributable to scatter is given by the following ratio: $\mu_{scat}(E)/\mu_T(E)$, where $\mu_{scat}(E)$ = the linear attenuation coefficient for both scatter processes. The dependency of scatter upon iodine concentration can be quickly determined by calculating the scatter linear attenuation coefficient near 30 keV, the approximate energy at which scattered photons will be detected, when iodine concentration is 10 mg/ml. This value for $\mu_{scat}(30)$ is equal to the sum of the mass attenuation coefficients for scatter for iodine and muscle multiplied by the appropriate concentrations:

$$\mu_{scat}(30) = \mu'_{Iscat}(30)\rho_I + \mu'_{Mscat}(30)\rho_M \qquad (2.16)$$

Using the values for the mass attenuation coefficients found in Hubbell [1982] and for the concentrations used in equation 2.13, $\mu_{scat}(30)$ is found to be:

$$\mu_{scat}(30) = 0.840\ (0.01) + 0.229\ (1.06) = 0.251\ cm^{-1} \qquad (2.17)$$

Based on this result, the contribution of expected iodine concentrations to scatter is on the order of only 3% of the total scatter and can therefore be considered a negligible influence.

Detection Rate of Background Radiation

The fraction of scattered photons which are deflected toward the detector is an important factor influencing the rate of detected scatter. This fraction is dependent upon the type of scatter and the angle at which the detector is oriented relative to the axis of the irradiating X-ray beam. The angular distribution of photons is also dependent upon the energy of the incident photons. Therefore, with each linear attenuation coefficient for coherent and incoherent scatter there is an associated function of angular distribution about the axis of irradiation which takes into account the energy of a photon and is given is units of the fraction of scattered photon intensity per steradian. This function is designated here as $f(\theta,E)$, where θ = the angle relative to the axis of the irradiating beam, and E = the energy of the photon.

Taking into account scattered photons' angular distributions and the energy loss due to incoherent scatter and following the derivation used for fluorescence detection rate, the rate at which a spectrum of scattered photons reaches a detector oriented 90° from the axis of irradiation per unit energy, call it $S_d(E)$, can now be written as:

$$S_d(E) = \Omega_d XYZ \left[\mu_{coh}(E)\, f_{coh}(90,E)\, I(E,0) + \right.$$
$$\left. + \mu_{incoh}(E_O)\, f_{incoh}(90,E_O)\, I(E_O,0) \right] \qquad (2.18)$$

where Ω_d = the solid angle subtended by the detector, XYZ = the size of the sensitive volume, $\mu_{(scat)}(E)$ = the linear attenuation coefficient for the

specified scatter process, $f_{(scat)}(90,E)$ = the fraction of photons distributed 90° per steradian for the specific scatter process, I(E,0) = the intensity of the irradiating beam, and E_O = the original energy of photons scattered incoherently as defined in equation 2.15.

Based on the above analysis, the result of equation 2.18 shows that the rate of background radiation detected at an energy of about 28.5 keV is constant for low iodine concentrations. And similar to the expression for the K_α photon detection rate, this expression also shows that the rate at which scattered photons will strike the detector is dependent upon the size of the sensitive volume, the solid angle subtended by the detector's crystal and the characteristics of the X-ray beam.

Estimation of Iodine Concentration from X-ray Fluorescence

Figure 2.2 shows an empirically determined plot of the rate of 28.5 keV photons detected over a range of low iodine concentrations. This plot represents the relationship found for a specific sensitive volume which was bounded by an X-ray beam of 7.1 mm^2 cross-sectional area and the detector's field-of-view of ~3 mm. Therefore, the sensitive volume was ~22 mm^3. The plot of figure 2.2 shows that the relationship between fluorescence and iodine concentration is linear for concentrations less than 5 mg/ml, although the linear approximation is still quite valid up to about 10 mg/ml as predicted by equation 2.14. It is also clear that background radiation is indeed detected when no iodine is present in the sensitive volume.

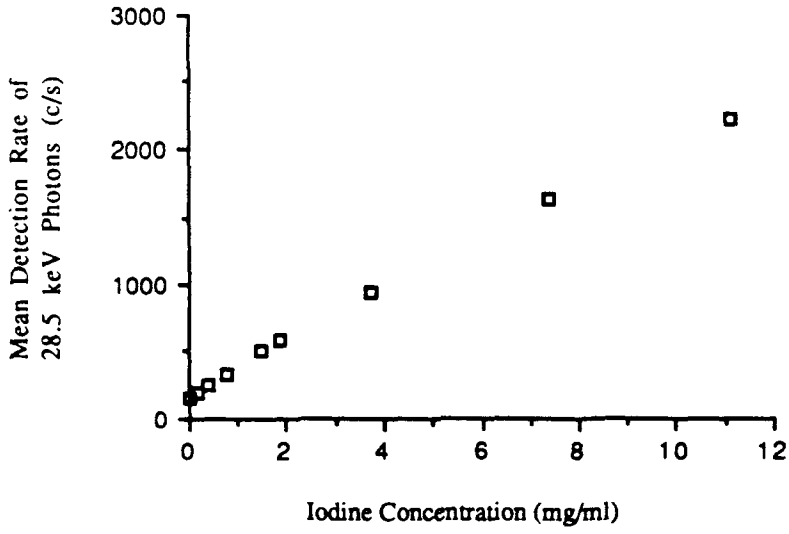

Figure 2.2: Empirically Determined Relationship between Fluorescence Detection Rate and Iodine Concentration. The relationship is shown to be approximately linear for iodine concentrations up to about 10 mg/ml. The detection rate at zero iodine concentration is equal to the rate of background radiation detected at 28.5 keV.

Figure 2.2 can be used as a calibration curve from which iodine concentration could be calculated based on the rate of 28.5 keV photon detection. This rate of 28.5 keV photon detection is equal to the sum of the rate of fluorescence detection and the rate of background detection. Let λ_d represent the total detection rate of 28.5 keV photons, λ_b represent the rate of background detection, and λ_f represent the rate of fluorescence detection, found earlier to be equal to the product of a constant times the iodine concentration, i.e. $\lambda_f = m\rho_I$. The relationship between detected rate and iodine concentration is then given as:

$$\lambda_d = \lambda_f + \lambda_b = m\rho_I + \lambda_b \tag{2.19}$$

To calculate the iodine concentration based on the rate of detection, simple algebra gives the following relationship:

$$\rho_I = (\lambda_d - \lambda_b)/m \tag{2.20}$$

In practice, however, it is necessary to estimate the detection rate based on a finite number of photons counted within a time interval T. The processes of photon emission and counting have been known to be random processes. Therefore, any calculation of iodine concentration using equation 2.20 will have some error associated with the estimation of the detection rate. In this way, the accuracy with which this rate can be determined directly affects the accuracy with which iodine concentrations are inferred. In order to quantitate the accuracy of iodine concentration estimates made using X-ray

fluorescence, the following statistical model of the counting process was examined.

Statistical Modeling of Concentration Estimators

A random process like the detection of photons emitted from a radiation source has been traditionally and successfully modeled as a Poisson process [Snyder 1975]. Modeling of this process begins by allowing a random variable N represent the number of photons counted over a time interval T when the mean detection rate of photons from the sample is λ_d. The random variable N has possible values which are all integers; therefore, the probability density function of N is defined as the probability that N is equal to an integer n:

$$Pr(N=n) = \frac{(\lambda_d T)^n e^{-\lambda_d T}}{n!} \tag{2.21}$$

The mean detection rate, λ_d, is equal to the sum the mean detected background rate (λ_b) and fluorescence rate (λ_f) and is a valid summation for this model when these two processes are independent, which is effectively the case at low iodine concentrations. As was shown earlier, there is also a linear relationship between the mean fluorescence rate and the concentration, i.e. $\lambda_f = m\rho_I$, where m is the linear proportionality constant. Therefore, the probability density function of equation 2.21 can be rewritten with the following substitution made, $\lambda_d = m\rho_I + \lambda_b$:

$$Pr(N=n) = \frac{(m\rho_I+\lambda_b)^n T^n e^{-(m\rho_I+\lambda_b)T}}{n!} \tag{2.22}$$

The most likely concentration to have produced any single observed count, call it n_0, is called the maximum likelihood estimate and is equivalent to the value of ρ_I that maximizes the likelihood function $L(\rho_I)$ which, for a single observation, is simply equal to the expression given in equation 2.22 with n = n_0 [Snyder 1975, p. 75; Hogg & Tanis 1983, p. 266]:

$$L(\rho_I) = \frac{(m\rho_I+\lambda_b)^{n_o}T^{n_o}\, e^{-(m\rho_I+\lambda_b)T}}{n_0!} \qquad (2.23)$$

The concentration which maximizes this expression will also maximize its natural logarithm; therefore, the maximum likelihood estimate, expressed here as $\hat{\rho}_I$, satisfies the equation:

$$\frac{\partial \ln L(\hat{\rho}_I)}{\partial \hat{\rho}_I} = \frac{\partial}{\partial \hat{\rho}_I} \{ n_0[\ln(m\hat{\rho}_I+\lambda_b) + \ln T] - (m\hat{\rho}_I+\lambda_b)T - \ln(n_0!) \} = 0 \qquad (2.24)$$

which simply is:

$$\frac{n_0 m}{m\hat{\rho}_I + \lambda_b} - mT = 0 \qquad (2.25)$$

and results in a maximum likelihood estimate of

$$\hat{\rho}_I = (\frac{n_0}{T} - \lambda_b)/m \qquad (2.26)$$

This result is in agreement with equation 2.20 where an estimate of the total detection rate, λ_d, is n_0/T.

Accuracy of Iodine Concentration Estimates

Now that the estimator of concentration has been defined, it is necessary to find the accuracy of this estimate. The accuracy can be defined in two ways; as the probability that any single estimate of concentration would be within some minimally acceptable range of the actual concentration present, or simply as the standard deviation of the estimate in units of concentration where a lower standard deviation would refer to higher accuracy. These two indices of accuracy are related, but the use of one as opposed to the other may be more appropriate for different situations. The following section will derive these accuracy indices from the Poisson model already presented and apply them to determine an index of overall system performance, the signal-to-noise ratio

Consider again the probability density function of the random variable N, as given in equation 2.22. Let this distribution of a discrete type random variable be approximated as a continuous type by allowing a Gaussian distribution to represent the probability density function (PDF) of N [Hogg & Tanis 1983, p. 251]:

$$PDF(N) = \frac{\exp[(n - (m\rho_I+\lambda_b)T)^2 / 2(m\rho_I+\lambda_b)T]}{\sqrt{2\pi}\sqrt{(m\rho_I+\lambda_b)T}} \qquad (2.27)$$

This representation of a discrete Poisson distribution as a continuous Gaussian distribution is valid for expected counts of $n > 20$, as would be the case for almost all X-ray fluorescence investigations.

The first task in determining the standard deviation of the estimate is to find the probability density function of the estimator random variable $\hat{P}_I$ which represents all possible estimators of a concentration and has elements of $\hat{\rho}_I$. The distribution PDF(N) must be transformed to describe the distribution of $\hat{P}_I$ using the following standard transformation method [Hogg & Tanis 1983, p. 258]:

$$PDF(\hat{P}_I) = |n'(\hat{\rho}_I)|\ PDF(n(\hat{\rho}_I)) \tag{2.28}$$

where $n(\hat{\rho}_I)$ is the function which relates the elements n and $\hat{\rho}_I$ by the substitution to be made, namely $\hat{\rho}_I = (n - \lambda_b T)/mT$. Therefore, $n(\hat{\rho}_I) = m\hat{\rho}_I T + \lambda_b T$, and $n'(\hat{\rho}_I) = mT$.

Utilizing the substitution rule given by equation 2.28 and the original function PDF(N) from equation 2.27, the function $PDF(\hat{P}_I)$ is found to be:

$$PDF(\hat{P}_I) = mT \frac{\exp\{(mT)^2 [\hat{\rho}_I - \rho_I]^2 / 2(m\rho_I+\lambda_b)T\}}{\sqrt{2\pi}\sqrt{(m\rho_I+\lambda_b)T}} \tag{2.29}$$

The mean of the random variable $\hat{P}_I$ is the actual concentration present, ρ_I, and the standard deviation of $\hat{P}_I$, call it σ_P, is $\sqrt{(m\rho_I+\lambda_b)T}\,/mT$. It should be clear that lower values for the standard deviation correspond to more accurate estimates. Therefore, the reciprocal of σ_P can be used as an index of accuracy.

The accuracy of an estimate can also be described by the probability that the estimate is within some range $\Delta\rho_I$ of the actual concentration present

and is quantitated as:

$$\Pr(\rho_I-\Delta\rho_I \le \hat{P}_I \le \rho_I+\Delta\rho_I) = \int_{\rho_I-\Delta\rho_I}^{\rho_I+\Delta\rho_I} PDF(\hat{P}_I)\, d\hat{\rho}_I \tag{2.30}$$

whose value can be represented with an error function:

$$\Pr(\rho_I-\Delta\rho_I \le \hat{P}_I \le \rho_I+\Delta\rho_I) = \text{erf}\left[\frac{mT\Delta\rho_I}{\sqrt{2(m\rho_I+\lambda_b)T}}\right] \tag{2.31}$$

Through the use of equation 2.31, the probability, or certainty, that any one estimate $\hat{\rho}_I$ is within some range $\Delta\rho_I$ of the actual concentration ρ_I can be calculated.

Although the accuracy of a single estimate can be quantitated with equation 2.31, it does not provide a conventional measure of the performance of the fluorescence technique. One conventional description of performance is the signal-to-noise ratio which is a particularly important quantity for dynamic signals. The signal-to-noise ratio (SNR) can be defined as the magnitude of the concentration present divided by the standard deviation of the estimate of that concentration:

$$SNR = \frac{\rho_I}{\sigma_\rho} = \frac{mT\rho_I}{\sqrt{(m\rho_I+\lambda_b)T}} \tag{2.32}$$

As can be seen from equation 2.32, the signal-to-noise ratio is proportional to the reciprocal of the standard deviation of the concentration estimator, an index of accuracy. In addition, the signal-to-noise ratio could be considered to be equal to the argument of the error function of equation 2.31 when the range $\Delta\rho_I$ is proportional to the concentration present, specifically $\Delta\rho_I = \sqrt{2}\,\rho_I$. Therefore, this definition of the signal-to-noise ratio is particularly well suited to describe the performance of an X-ray induced fluorescence system.

The definition of signal-to-noise ratio as given by equation 2.32 was used in the present work as a guide for the optimization of the X-ray fluorescence system. This parameter was also valuable in determining the requirements of future systems, although slight modifications of equation 2.32 were necessary.

Chapter 3

X-RAY FLUORESCENCE SYSTEM

Some of the first applications of the X-ray induced fluorescence of iodine *in vivo* were performed by Hoffer [1969] to measure iodine concentration in the thyroid gland. An americium-241 source was used to induce the fluorescence of iodine which had accumulated in the thyroid after its intravenous injection, and a concentration map was made which facilitated diagnosis of thyroid pathologies [Hoffer et al. 1971]. Studies of iodine kinetics *in vivo* have also been performed using a similar system. Estimates of kidney function have been assessed by monitoring the clearance of iodine from the blood pool after the administration of an iodinated contrast agent in rabbits [Sjoberg et al. 1981] and in humans [Grönberg et al. 1983]. Hepatic function has also been studied by measuring iodine concentrations of the liver, blood and bile [Koehler et al. 1976].

Measurements of blood flow, more specifically cerebral blood flow [Ter-Pogossian et al. 1971; Phelps et al. 1973] and cardiac output [Kaufman et al. 1972], have also been performed using X-ray fluorescence of an iodinated tracer injected peripherally. With the use of more intense X-ray beams, provided by conventional X-ray generators, the fluorescence rate of iodine was dramatically increased. This increase in source beam intensity was considered necessary for monitoring iodine transients deep inside the thorax or the skull due to their attenuation of fluorescence photons. With the use of these more intense X-ray beams, radiation dose became a concern. However,

the radiation dose imparted to the subject was found to be acceptable, particularly due to its being localized to the region under investigation [Ter-Pogossian et al. 1971; Kaufman et al. 1972].

The X-ray fluorescence system developed in the present work is similar in design to that used by Ter-Pogossian et al. [1971], Kaufman et al. [1972], and Phelps et al. [1973]. The system was designed to monitor the iodine concentrations in the myocardium, the region where perfusion is to be determined, and at the origin of the coronary artery supplying blood to that portion of the myocardium. The origin of the coronary arteries is the ostium of the coronaries in the aorta, but if we assume that the iodine concentration in the left ventricular lumen is not appreciably different from that at the ostium, then monitoring iodine concentration in the left ventricular lumen suffices as the origin of the coronary arteries in this capacity.

This chapter describes the X-ray fluorescence system which was developed to monitor and record iodine concentration transients in the left ventricular lumen and in the region of interest in the myocardium. After an initial description of the hardware which was available for this prototype system, the optimization of system performance is discussed. And finally, the specific attributes of X-ray fluorescence system utilized in this work, such as spatial resolution and signal-to-noise ratio, are reported.

Hardware and Basic Design

The hardware available for this fluorescence system were the following: an X-ray generator, a high purity Germanium (Ge) photon detector, a Sodium-Iodine (NaI) photon detector, a specific collimator for each detector, necessary electronics to identify the energy of photons which strike the detectors' crystals, and a laboratory computer. The typical utilization scheme for these components is described below.

The X-ray generator (General Electric MSI-1250) was capable of providing X-ray photons of an energy spectrum bounded by a maximum potential of 125 kVp. The intensity of the beam could be controlled by setting the current run through the generator. For the purpose of irradiating a target with a narrow X-ray beam, it was necessary to collimate the beam such that the beam has a small circular cross-section. The actual settings of the generator and the filtering of the beam which provided an optimal X-ray source are discussed in the next section.

The Ge detector (Aptec model #PS510-F3C) was fitted with a collimator which had a field of view restricted to a width of ~3 mm at a focal length of 12 cm from the collimator. The field of view of the collimator for the NaI detector (Gull Eng.) encompassed ~6 mm also at 12 cm from the collimator. The Ge detector was chosen to monitor the myocardium due to its comparatively smaller sensitive volume which provided better spatial resolution.

Both the Ge and NaI detectors operate under similar principles. Upon the incidence of an X-ray photon, the detector produces an electric pulse of a voltage proportional to the photon's energy. The pulses are amplified and shaped by external circuitry (EG&G ORTEC models #673 and #474) and are then routed to single channel analyzers (EG&G ORTEC model #551) for energy discrimination. Those pulses corresponding to 28.5 keV are selectively routed to ratemeters (EG&G ORTEC model #449) whose output voltage reflects the frequency of X-ray photons detected at that energy. Therefore, monitoring the ratemeters associated with each detector provided a measure of the iodine concentrations in the respective regions of interest in the heart. A laboratory computer (Tektronix Terminal 4051) retrieved the data recorded by an analog-to-digital converter (Tektronix Digital Oscilloscope 2230) which sampled the ratemeters continuously at 10 Hz. Analysis of the tracer transients was then performed off-line with a mainframe computer (DEC VAX 11/780).

Optimization of X-ray Fluorescence System

Optimizing the performance of an X-ray fluorescence system entails maximizing the signal-to-noise ratio. From the definition of signal-to-noise ratio given in equation 2.31, the index followed for the optimization of the X-ray fluorescence system is written as:

$$SNR(\rho_I) = \frac{m\rho_I\sqrt{T}}{\sqrt{m\rho_I+\lambda_b}} \qquad (3.1)$$

where m = the slope of the calibration curve relating fluorescence to iodine

concentration, ρ_I = iodine concentration, T = interval over which counting is done, and λ_b = rate of background radiation detected in the energy range of the fluorescence photons. Some important features of this quantity are its dependence upon the slope of the calibration curve, the background radiation, the counting time interval, and even the iodine concentration. Because iodine concentration is the only term which is not system dependent, the signal-to-noise ratio is given here as a function of iodine concentration, ρ_I.

It is obvious from equation 3.1 that an increase in the amount of time allowed for analysis will improve the accuracy of any estimate of concentration. However, there were time constraints imposed here due to the fact that concentration transients must be sampled at intervals dictated by the Nyquist digital sampling criterion. The sampling period was set here to 0.1 seconds. However, because the sampling was continuous, i.e. each sample was taken immediately after the preceding one, the time interval T will be reported here as the fraction of time when counting occurs. For the system which samples continuously, T = 1. This designation of the time interval is useful when comparing future systems which may be gated to count photons only within certain intervals of the cardiac cycle.

The term m is the proportionality constant which relates the detection rate of fluorescence with iodine concentration. The many factors which influence this value are described explicitly in equation 2.14 and include the incident beam's energy spectrum, the incident beam's intensity, the solid angle subtended by the detector's crystal, and the size of sensitive volume.

These factors similarly define the rate of background radiation detection, and therefore λ_b, according to the expression given by equation 2.17. The properties of the incident X-ray beam certainly are factors which can be modified in order to optimize the values of m and λ_b.

Other factors which influence the terms m and λ_b are the detector's resolution and the window of the energy spectrum over which counting is observed. Figure 3.1 shows a close-up of the spectrum around 28.5 keV as detected by the Germanium photon detector. Although the fluorescence photons arrive at the detector's crystal at very precise energies, the detector will perceive the energy of each photon with some error. This error is reflected in the energy spectrum as a distribution about the actual photon energy. The standard deviation of this distribution is dependent upon the detector and can be represented as σ_E.

Because there is a distribution of energies which correspond to the fluorescence photons, some range of energies about 28.5 keV must be used for photon counting. That portion of the spectrum which is monitored for counting is called the counting window. An example of a counting window is depicted in figure 3.1 where the minimum and maximum energies which bound the window are termed E_{min} and E_{max}, respectively. Utilization of an optimal counting window is of interest and is addressed here first.

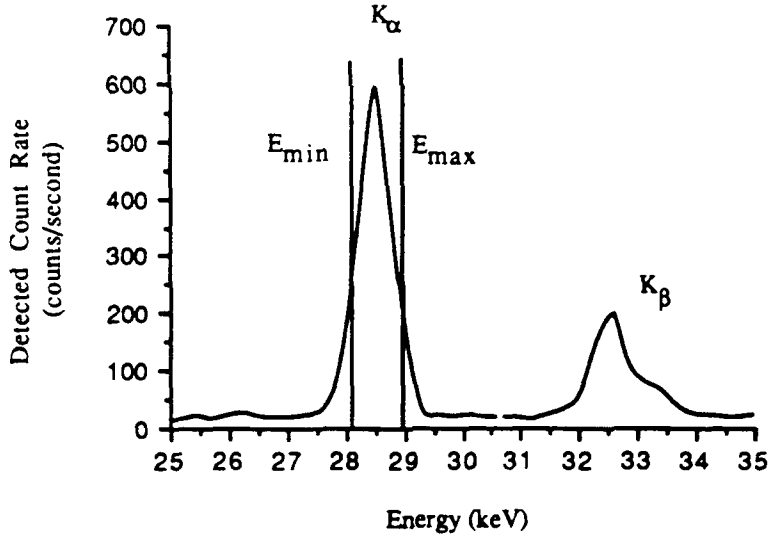

Figure 3.1: Detected Energy Spectrum of Photons in the Range of 25-35 keV Emitted from an Irradiated Sample Containing Iodine. The broadening of the peaks are due to limits in the detector's energy resolution. The energies bounded by Emin and Emax represent the window within which photons are counted.

Optimal Counting Window

In consideration of the counting window, the rate of detected background photons, λ_b, over the range E_{min} and E_{max} is given as:

$$\lambda_b = \int_{E_{min}}^{E_{max}} S_d(E)\, dE \qquad \text{(counts/second)} \tag{3.2}$$

where $S_d(E)$ represents the distribution of background radiation expressed by equation 2.17. As stated earlier, the characteristics of $S_d(E)$ are very much dependent upon the incident energy spectrum and apparatus geometry which dictates the contribution of coherent and incoherent scattering.

The value of m is equivalent to the detected count rate of fluorescence photons per unit concentration. Expressed mathematically:

$$m = \int_{E_{min}}^{E_{max}} X_{K\alpha}(E)\, dE \qquad \left(\frac{\text{counts/second of detected } K_\alpha \text{ photons}}{\text{unit concentration of iodine}}\right) \tag{3.3}$$

where $X_{K\alpha}(E)$ represents the energy distribution and rate of detection of the K_α photons.

In order to find the optimal counting window with the values for m and λ_b defined above, their influence on the signal-to-noise ratio given by equation 3.1 must be investigated. However, it should be noted that the signal-

to-noise ratio is a function of iodine concentration. One concentration should be chosen to allow for valid comparisons. Because very low concentrations of iodine are expected, the signal-to-noise ratio at $\rho_I = 0$ might be useful; however, by definition SNR(0) = 0. Therefore, for the purpose of determining the optimal counting window, the derivative of SNR(ρ_I) with respect to ρ_I evaluated at $\rho_I = 0$ will be used here and is given as:

$$SNR'(0) = \frac{m\sqrt{T}}{\sqrt{\lambda_b}} = \frac{\int_{E_{min}}^{E_{max}} X_{K\alpha}(E)\, dE}{\sqrt{\int_{E_{min}}^{E_{max}} S_d(E)\, dE}} \qquad (3.4)$$

where T is taken to be equal to 1 for this calculation, a condition which does not effect on the optimal E_{min} and E_{max}.

In order for this expression to be useable for optimization purposes, some assumptions about the distributions $S_d(E)$ and $X_{K\alpha}(E)$ must be made. For simplicity, consider $S_d(E)$ to have a constant value b over the entire range of the peak $X_{K\alpha}(E)$. The integral of $S_d(E)$ is then symmetric about the mean of $X_{K\alpha}(E)$, call it $\hat{E}$, and simply becomes:

$$\int_{E_{min}}^{E_{max}} S_d(E)\, dE = \int_{E_{min}}^{E_{max}} b\, dE = 2b(E_{max}-\hat{E}) \qquad (3.5)$$

The energy distribution of $X_{K\alpha}(E)$ can be modeled as a Gaussian distribution having a mean equal to the K_α photons energy, $\bar{E} = 28.5$ keV, and a standard deviation, σ_E. If the total rate of characteristic photons detected from a unit concentration is $K_{\alpha d}$, described by equation 2.14, then $X_{K\alpha}(E)$ can be represented as:

$$X_{K\alpha}(E) = \frac{K_{\alpha d}}{\sqrt{2\pi}\,\sigma_E} \exp\left[\frac{-(E-\bar{E})^2}{2\sigma_E{}^2}\right] \tag{3.6}$$

The evaluation of the definite integral of $X_{K\alpha}(E)$ is facilitated by allowing the variable E to be substituted by $x = (E-\bar{E})/\sigma_E$. The integral is then given as:

$$\int_{E_{min}}^{E_{max}} X_{K\alpha}(E)\,dE = \int_{E_{min}}^{E_{max}} \frac{K_{\alpha d}}{\sqrt{2\pi}\,\sigma_E} \exp\left[\frac{-(E-\bar{E})^2}{2\sigma_E{}^2}\right] dE = 2K_{\alpha d} \int_{0}^{x_{max}} \frac{1}{\sqrt{2\pi}} \exp\left[\frac{-x^2}{2}\right] dx \tag{3.7}$$

where x_{max} is directly related to half of the total width of the counting window by $x_{max} = (E_{max}-\bar{E})/\sigma_E$. If the substitution $x = (E-\bar{E})/\sigma_E$ is also used in the expression for the background radiation, then the index SNR'(0) becomes:

$$SNR'(0) = \frac{2K_{\alpha d} \int_{0}^{x_{max}} \frac{1}{\sqrt{2\pi}} \exp\left[\frac{-x^2}{2}\right] dx}{\sqrt{2b\,\sigma_E\,x_{max}}} = \frac{\sqrt{2}K_{\alpha d}}{\sqrt{b\sigma_E}} \frac{\int_{0}^{x_{max}} f(x)\,dx}{\sqrt{x_{max}}} \tag{3.8}$$

where the function f(x) is used to represent the Gaussian distribution with a mean of 0 and a standard deviation of 1.

It is clear from equation 3.8 that optimizing the energy window requires maximizing the ratio $\int_0^{x_{max}} f(x)dx \,/\, \sqrt{x_{max}}$. Using standard mathematical tables, this ratio has a maximum value of .3453 when $x_{max} = 1.4$. The result $x_{max} = 1.4$ corresponds to a total energy window of $2(E_{max}-\dot{E}) = 2.8\,\sigma_E$. Because the full-width-half-max (FWHM) value of a peak under investigation is equal to $2.355\,\sigma_E$, the optimal energy window width, call it E_W, is given as:

$$E_W = 2.8\,\sigma_E = 1.2\,\text{FWHM} \tag{3.9}$$

Although this value of E_W may be optimum, it should be pointed out that a decrease in SNR'(0) greater than 5% does not occur for values of E_W within the range of 0.81 - 1.71 FWHM.

If the optimal window is being utilized, the index SNR'(0) is given as:

$$SNR'(0) = 0.5\,\frac{K_{\alpha d}}{\sqrt{b\sigma_E}} \tag{3.10}$$

where $K_{\alpha d}$ = the total detection rate of fluorescence photons, b = the rate of background radiation detected per keV, and σ_E = the standard deviation of the distribution of detected K_α photons. In general, the ratio $K_{\alpha d}/\sqrt{b\sigma_E}$ can be used as a guide for the optimization of any X-ray fluorescence system meant to monitor very low concentrations. The term σ_E is dependent upon the detector being used; the other terms, $K_{\alpha d}$ and b, are dependent upon other factors, such as beam characteristics, which are discussed in the next section.

Optimal Beam Characteristics

Using an appropriate X-ray source is an important concern for maximizing the rate of fluorescence and minimizing background. An ideal incident beam would efficiently produce electron orbit vacancies while reducing scatter radiation of energies near the energy of fluorescence photons. However, the strategy which dictates the choice of X-ray spectrum is not so much dependent upon the signal-to-noise ratio as it is dependent upon factors such as photon penetration and minimum radiation dose.

The beam must be able to penetrate a closed thorax without excessive attenuation. High energy photons are therefore required and are delivered optimally when the X-ray generator is set at 125 KVP. Certainly, higher beam intensities will provide more fluorescence, and, although this also means an increase in background, the signal-to-noise ratio is maximized with the maximum beam intensity. Therefore, the X-ray generator's optimal intensity setting is its maximum, 5 ma for the machine used in this work.

Further modification of the energy spectrum can be accomplished by filtering the source. Filtering the beam with a relatively low atomic numbered element, such as copper, will prevent X-ray photons of low energies, in the range of 10-30 keV, from irradiating the subject. Because these low energy photons will not penetrate the thorax, and will therefore only contribute to radiation dose and background radiation, filtering the radiation source with 10 mils of copper was considered appropriate.

Prototype X-ray Fluorescence System

Figure 3.2 illustrates schematically the final dimensions and relative positions of the important features of the fluorescent system used for monitoring iodine concentrations with the X-ray fluorescence system. The X-ray source is a conventional X-ray generator set to 125 kVp and 5 ma. The beam is filtered with 10 mil Cu, cylindrically collimated to a diameter of ~3 mm and aimed horizontally to irradiate simultaneously the left ventricular lumen and the left ventricular free wall. The detectors which monitor the iodine fluorescence in these two regions are positioned over the subject.

Spatial Resolution

Spatial resolution refers to the size of the sensitive volume which is being monitored for iodine content and is reported here as the full-width-half-max (FWHM) of the point spread functions defining the sensitive volume. With this fluorescence system, a sensitive volume is defined by the cross-section of the X-ray beam and the linear field of view of the detector along that beam. Because of the proximity of the two detectors relative to the their distance from the beam source, the beam's cross-section is considered equal for both sensitive volumes in the present X-ray fluorescence system. The beam was collimated to a FWHM diameter of 3 mm; therefore, the area which is effectively irradiated by the beam is $\pi(1.5)^2 = 7.1\ mm^2$.

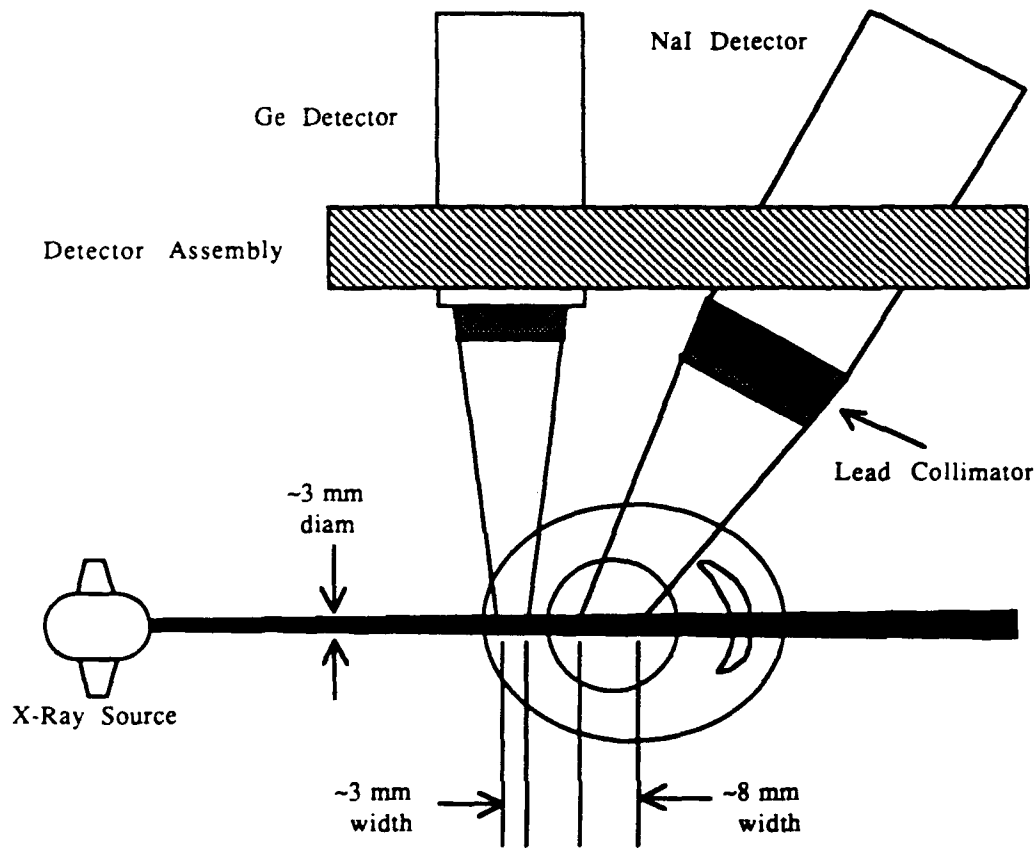

Figure 3.2: Schematic of X-ray Fluorescence System and Its Positioning Relative to Subject's Heart.

The point spread function for the Ge detector's field of view has a FWHM of 3 mm. In conjunction with the information about the beam's cross-section, this shows the sensitive volume of the Ge detector to be about $\pi(1.5)^2$ mm^2 x 3 mm $\approx$ 22 mm^3. The field of view of the NaI detector was known to be collimated to a FWHM of 6 mm; however, the angle at which it is positioned in the detector assembly increases this width. The point spread function along the beam's axis was found to have the FWHM of ~8 mm. Therefore, the effective sensitive volume of the NaI detector was $\pi(1.5)^2$ mm^2 x 8 mm $\approx$ 56.8 mm^3.

Signal-to-Noise Ratios

The signal-to-noise ratio is a measure of the performance of the X-ray fluorescence system and is expressed quantitatively by equation 3.1 as:

$$SNR(\rho_I) = \frac{m\rho_I\sqrt{T}}{\sqrt{m\rho_I+\lambda_b}} \qquad (3.11)$$

The $SNR(\rho_I)$'s for both the Ge and NaI detectors under conditions described above, including when T = 1, are shown in figure 3.3. The most noteworthy difference between these functions is the fact that the SNR of the NaI detector is substantially higher than that for the Ge detector for all iodine concentrations. This discrepancy is due to the NaI detector's larger sensitive volume and substantially larger crystal area.

The Ge detector does produce more accurate measurements in the smaller sensitive volume, however, particularly of low concentrations of

iodine (~0-2 mg/ml) which are expected in the myocardium. Figure 3.4 shows a plot of the SNR(ρ_I) for both detectors when their sensitive volumes are of equal size. Based on the plots shown in figure 3.4, the use of the Ge detector is justified when good spatial resolution and accurate measurements of low concentrations are necessary. The value of the signal-to-noise ratio for the Ge detector at an iodine concentration of 1 mg/ml, SNR(1) = 11.7, should be noted here because it is used in Chapter 6 as a minimally tolerable value for this and future systems.

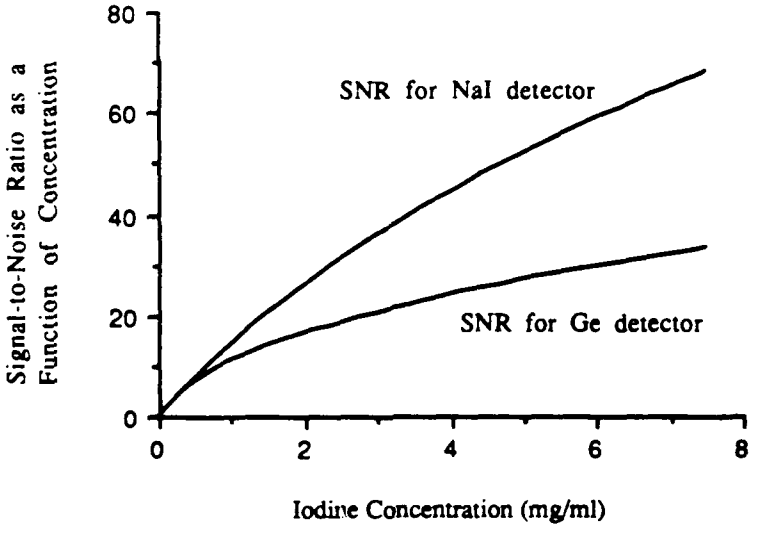

Figure 3.3: Signal-to-Noise Ratio Functions for Each Detector. The signal-to-noise ratio of the NaI detector is much greater than that of the Ge detector and is due to the differences in their sensitive volumes and crystal areas.

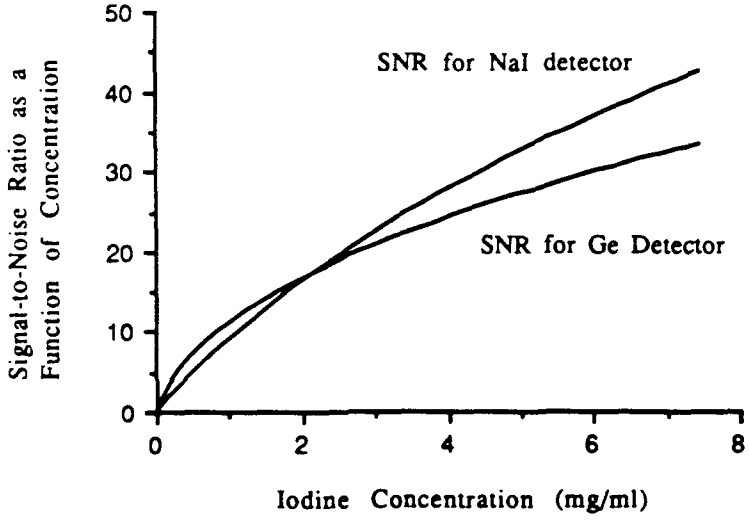

Figure 3.4: Signal-to-Noise Ratio for Each Detector Monitorring the Same Sized Sensitive Volume. As can be seen here, the signal-to-noise ratio of the Ge detector is slightly greater than that of the NaI detector for iodine concentrations less than about 2 mg/ml.

Chapter 4

SIGNAL ANALYSIS

Techniques designed to measure regional myocardial perfusion must not only be able to record accurately a tracer's concentration and distribution, but the technique must also be capable of applying that tracer data to a valid model relating tracer transport to blood supply. Two types of models are currently of practical use; one relating tissue uptake of a tracer to blood supply and the other relating dynamic characteristics of tracer transport to blood flow. Techniques which employ this latter group of models are referred to collectively as indicator-dilution methods.

Because the iodinated tracer used in this study does not accumulate in intracellular space, a model of tracer kinetics was examined in order to calculate perfusion from the recorded iodine concentration transients. This chapter will focus on the development of a model of tracer transport and the methods used for calculating characteristics of tracer transport from which blood flow can be inferred.

Introduction to Indicator-Dilution Methods

Indicator-dilution methods have been used for measuring various characteristics of biological transport phenomena, such as flow rates, organ blood volume and membrane permeabilities. The acceptability and subsequent success of indicator-dilution methods arose from the simple concept on which

it is based; any substance which can be detected without disturbing the system of interest can be introduced into that system and its transport monitored such that conclusions about transport mechanisms can be made.

The first reported use of indicator-dilution *in vivo* was performed by Stewart [1897] for measuring cardiac output. The technique required the injection of the tracer, a NaCl solution, either in the right heart or in the left ventricle. A catheter was placed in the aorta for blood withdrawal during the time when tracer concentration was most evident. This time interval was recognized by the ringing of a telephone which was activated by the increased electrical conductance of the blood in the aorta which was monitored by electrodes on the vessel.

Figure 4.1 shows a typical indicator-dilution curve that would be expected to appear in the aorta after a right heart injection of the tracer. Although Stewart [1897] was unable to record the tracer's concentration transient, he did experience the transient loudness of the bell's ringing which was proportional to the concentration of the NaCl solution as it passed through the aorta. The collection of the blood during the ringing period allowed him to estimate the aortic concentration time integral, a quantity inversely proportional to the cardiac output.

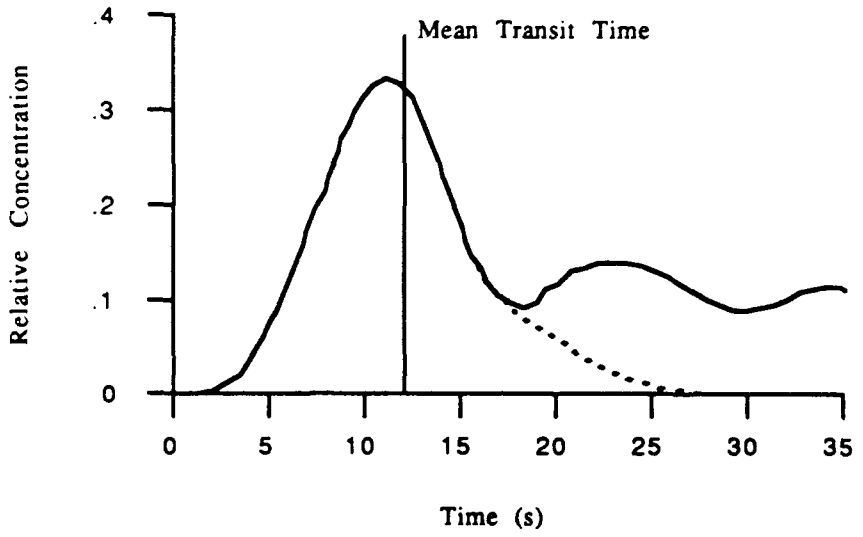

Figure 4.1: A Typical Indicator-Dilution Curve. This indicator-dilution curve is one which would be expected in the aorta after a right heart bolus injection of indicator. The extrapolated first pass transient is shown, and its mean transit time is indicated.

A complementary set of experiments was performed later by Stewart [1921] after recognizing the importance of the tracer's arrival time at the aorta. He reasoned that the mean time for the tracer to reach the aorta from the right heart would be dependent upon the cardiac output and the volume of blood vessels through which the tracer must pass between these points. Using a technique similar to that for measuring cardiac output, Stewart [1921] estimated the mean transit time of the tracer's passage from the right heart to the aorta, and he was then able to calculate the volume of blood in the pulmonary vasculature. The mean transit time has since been recognized as an important characteristic of an indicator-dilution curve and is also shown for the indicator-dilution curve in figure 4.1.

The success of these and other early physiologic experiments can be attributed to the use of two equations which were viewed as qualitatively "obvious" relationships, obvious at least to the proponents of the techniques. The earliest quantitative arguments in favor of the relationships between flows, volumes and circulation times came from Hamilton et al. [1932]. Thereafter, the so-called Stewart-Hamilton equations have been the basis of many biological transport investigations. The first Stewart-Hamilton equation can be expressed as follows:

$$\text{Flow} = \frac{m}{\int_0^\infty c(t)\,dt} \qquad (4.1)$$

where m = amount of tracer injected, and c(t) = tracer concentration transient.

The second Stewart-Hamilton equation is given as:

$$\text{Volume} = \text{Flow} \times \text{Mean transit time} = \text{Flow} \times \frac{\int_0^\infty t\, c(t)\, dt}{\int_0^\infty c(t)\, dt} \qquad (4.2)$$

A rigorous derivation of the Stewart-Hamilton equations was finally presented by Meier and Zierler [1954] in a paper which essentially paved the way for modeling tracer transport and quantitating transport mechanisms based on indicator-dilution curves.

As could be expected, various different models have been developed to describe any one particular transport mechanism under investigation. However, many of the models used to calculate blood flow from tracer kinetics face nontrivial obstacles in their practical application. Some models rely on interpolating first pass transients which can be distorted by recirculation of the tracer. Still other problems may include relating the analysis of indicator-dilution curves to parameters of physiological significance, or the ambiguous representation of a tracer's input distribution, say at the injection site, being applied to transport models.

One particularly popular and successful solution to the recirculation problem relies on approximating first pass transients with a known function. An exponential decay function, for example, has been used to restore the tail of the first pass transient, like that the one shown in figure 4.1, and thereby

facilitate the calculation of the integral under the first pass transient and the mean transit time [Kinsman et al. 1929; Newman et al. 1951]. More recently, it has been suggested that the first pass transient, c(t), be represented as a gamma-variate function which can be written in the following form:

$$c(t) = \frac{t^{\alpha} e^{-t/\beta}}{\beta^{(\alpha+1)}\Gamma(\alpha+1)} \qquad (4.3)$$

where α and β are the calculable parameters, and $\Gamma(\alpha+1)$ is the gamma function. The suggestion of using a gamma-variate to represent first pass transients was based purely on the function's ability to accurately fit empirical data [Evans 1959; Thompson et al. 1964]. The gamma-variate approximation to the first pass transient has since been proven to be extremely effective in this role, particularly for determining cardiac output [Starmer & Clark 1970; Yoder & Swan 1971].

Utilization of the gamma-variate approximation has since been substantiated by demonstrating that the gamma-variate is a solution to standard mathematical models of tracer transport. Various compartmental models [Thompson et al. 1964; Schlossmacher et al. 1967; Davenport 1983] and a convection-dispersion model [Harpen & Lecklitner 1984] have all yielded the gamma-variate solution under the condition that the distribution of tracer at the site of injection is a spatial delta function. Based on the ability of the gamma-variate to fit empirical data, the assumption of a spatial delta function as an initial condition can be considered appropriate for many applications. Those specific conditions under which the spatial delta function assumption is

valid have been quantitated by Harpen & Lecklitner [1984].

One concern associated with the gamma-variate solution, however, is the physiological interpretation of the parameters which characterize the function. Through a compartmental model, Davenport [1983] was able to show that the two parameters, α and β of equation 4.3, could be interpreted as the number of mixing compartments minus one and the ratio of compartmental volume to flow rate, respectively. Based on this interpretation, the mean transit time of a first pass, which is predicted by the compartmental model to be equal to $(\alpha+1)\beta$, is in agreement with the value established by Meier and Zierler [1954]. Although the product of the gamma-variate parameters can be used in this context, the physiological significance of either one of these parameters by itself is not clear, as pointed out earlier by Harris and Newman [1970]. Furthermore, the gamma-variate solution presented by Davenport [1983] is dependent upon the term β remaining constant for all vessel types, a requirement which is neither analytically nor intuitively justifiable.

In response to these difficulties, flow studies using the gamma-variate fit to the first pass transient have not attached physiological significance to the associated parameters, but employed the gamma-variate fit simply for the convenience it provided in calculating the area under the first pass transient as well as the tracer's mean transit time [Carlsen & Hedegaard 1987; Jaschke et al. 1987; Hackländer et al. 1988]. Other stategies to calculate the mean transit time without curve fitting have also been developed and rely on exploiting the apparent linear properties of tracer transport through the circulatory system.

Transport of tracer through the circulation has been shown by Bassingthwaighte & Ackerman [1967] to have the properties of a linear system for which the system's impulse response, which is found by deconvolving the recorded outflow (or distal) transient with the inflow (proximal) transient, can be used to find characteristics of tracer transport, including the mean transit time. Some recent investigations of blood flow have relied on calculating the impulse response and its mean transit time using various deconvolution techniques [Coulam et al. 1966; Maseri et al. 1970; Nakai 1981; Wolpers et al. 1984]. Although the results of these latter flow studies employing the impulse response have been satisfactory, no theoretical model of tracer transport was offered to support the use of equation 4.2 with the methods used to find the mean transit time.

The remainder of this chapter presents a method for analyzing indicator-dilution curves which yields mean transit times while alleviating the problems outlined above. A theoretical representation of tracer transport is first developed with the convection-dispersion equation, and the parameters represented by the mean transit time of the impulse response are shown to agree with equation 4.2, the second Stewart-Hamilton equation. It is also shown that frequency domain analysis of indicator-dilution curves [Hays et al. 1967], similar to Fourier analysis presented by Coulam et al. [1966], will produce the mean transit time and other characteristics of tracer transport regardless of tracer recirculation, injection site and bolus shape. Consideration of multiple branching vessels and the practical aspects of using this method on biological indicator-dilution curves are also discussed.

Convection-Dispersion Model of Tracer Transport

The one-dimensional convective-dispersive model has been shown to accurately represent the transport of a tracer through various vessel types which can be loosely classified as representative of either cylindrical pipes or packed beds [Harris & Newman 1970]. Transport of tracers through cylindrical pipes with laminar, or steady, flow has been shown to be adequately represented by one-dimensional convective-dispersive transport under certain conditions, most notably the tracer's being sufficiently dispersed axially at the points of observation [Taylor 1953; Taylor 1954; Aris 1956]. Because flows through portions of major arteries, for example the circumflex artery, have been shown to elicit quasi-steady behavior which approximates laminar flow [Kajiya et al. 1985], the conditions under which the convection-dispersion transport can be considered valid are conceivably met by these arteries, subsequent arterioles and the venous system of the coronary vasculature.

Transport of several types of tracers through packed beds, as would be found at the level of the capillaries, has also been represented by the convective-dispersive model as suggested by Perl and Chinard [1968]. However, the convection-dispersion representation of tracer transport through capillary beds has been shown to be valid only for tracers which are extravascular, i.e. tracers which diffused across capillary walls, but not intracellular space [Perl & Chinard 1968; Leonard & Jorgensen 1974; Lenhoff & Lightfoot 1984]. Therefore, because the present work employed a tracer which

is extravascular according to the above definition, the following convection-dispersion model was considered valid.

The convection-dispersion equation representing tracer transport through a single vessel between a point x_0 and ∞ is given as:

$$\frac{\partial C}{\partial t} + Q\frac{\partial C}{\partial x} - D\frac{\partial^2 C}{\partial x^2} = 0 \qquad (4.4)$$

where $C = C(x,t)$, the mean tracer concentration over the cross-section of the vessel, x = the dimension along the axis of the vessel in units of volume, t = time, Q = mean flow rate of blood through the vessel, and D = effective diffusivity coefficient. Previous theoretical considerations of this equation included specifying an initial condition, such as a spatial delta function [Harpen & Lecklitner 1984]. For the model used in the present work, a boundary condition at x_0 is applied; therefore, there is no need to assume anything about sources of tracer upstream of x_0, including recirculation sources. The boundary condition at x_0 is given as:

$$C(x_0,t) = f(t) \qquad (4.5)$$

where $f(t)$ is a known function which might represent the concentration transient recorded at the inlet artery of an organ. Any concentration time transient downstream of x_0 can now be represented by the solution to equation 4.4 in accordance with the boundary condition stipulated by equation 4.5.

Using the Fourier transform defined as follows:

$$\boldsymbol{C}(x,\omega) = \int_{-\infty}^{\infty} C(x,t)\, e^{-j\omega t}\, dt \qquad (4.6)$$

equation 4.4 can be written as follows:

$$j\omega \boldsymbol{C} + Q\frac{\partial \boldsymbol{C}}{\partial x} - D\frac{\partial^2 \boldsymbol{C}}{\partial x^2} = 0 \qquad (4.7)$$

Equation 4.7 is an ordinary differential equation whose general solution is:

$$\boldsymbol{C}(x,\omega) = A_\zeta(\omega)\, e^{x\zeta(\omega)} + A_\eta(\omega)\, e^{x\eta(\omega)} \qquad (4.8)$$

with $\zeta(\omega) = \frac{Q}{2D} - \left(\frac{Q^2}{4D^2} + \frac{j\omega}{D}\right)^{1/2}$ and $\eta(\omega) = \frac{Q}{2D} + \left(\frac{Q^2}{4D^2} + \frac{j\omega}{D}\right)^{1/2}$

Because the net transport of tracer is downstream, and because tracer concentrations in biological systems do ultimately reach steady states, the system must be assumed to be causal and stable, respectively. Therefore, $\boldsymbol{C}(x,\omega)$ must be finite for all values of ω, and the term with $\eta(\omega)$ in the exponent is not an allowed solution, i.e. $A_\eta(\omega)$ must be equal to zero. The remaining term $A_\zeta(\omega)$ is defined by the boundary condition at $x = x_0$, $\boldsymbol{C}(x_0,\omega)$, which is the Fourier transform of f(t), of equation 4.5:

$$\boldsymbol{C}(x_0,\omega) = \boldsymbol{F}(\omega) = A_\eta(\omega)\, e^{x_0\eta(\omega)} \qquad (4.9)$$

This boundary condition defines $A_\zeta(\omega)$ as follows :

$$A_\zeta(\omega) = \boldsymbol{F}(\omega)\, e^{-x_0\zeta(\omega)} \tag{4.10}$$

Therefore, the solution for $\boldsymbol{C}(x,\omega)$ over the interval $x_0 \le x \le \infty$ is found to be:

$$\boldsymbol{C}(x,\omega) = \boldsymbol{F}(\omega)\, e^{(x-x_0)\zeta(\omega)} \tag{4.11}$$

The term $\boldsymbol{C}(x,\omega)$ of equation 4.11 represents the Fourier transform of the expected concentration transient at a point x based on the concentration transient recorded proximally at point x_0. With this equation, a concentration transient recorded anywhere along the vessel distal to x_0 can be used to characterize the transport through the vessel up to that point. As an example, consider the transient g(t) recorded at a point x_1 downstream of x_0. The Fourier transform of g(t), $\boldsymbol{G}(\omega)$, would be equivalent to $\boldsymbol{C}(x_1,\omega)$ in equation 4.11. The functions $\boldsymbol{G}(\omega)$ and $\boldsymbol{F}(\omega)$ are then related as:

$$\boldsymbol{G}(\omega) = \boldsymbol{F}(\omega)\, e^{(x_1-x_0)\zeta(\omega)} \tag{4.12}$$

The ratio $\boldsymbol{G}(\omega)/\boldsymbol{F}(\omega)$, call it $\boldsymbol{H}(\omega)$, characterizes the transport of tracer between the points x_0 and x_1 and is defined as:

$$\boldsymbol{H}(\omega) = e^{(x_1-x_0)\zeta(\omega)} \tag{4.13}$$

The function $H(\omega)$ is called a transfer function and is equivalent to the Fourier transform of the impulse response of the linear system represented by the convection-dispersion equation. The transfer function can be used to find tracer transport characteristics between the points x_0 and x_1, including the mean transit time of the impulse response which is defined as the first moment of the impulse response divided by its zeroeth moment [Meier & Zierler 1954]. These moments are calculated from the transfer function by making use of the moment theorem, which states that the each moment of the impulse response is proportional to its respective order derivative of the transfer function [Papoulis 1977, p. 66]. The mean transit time of the impulse response is then found directly from the transfer function as:

$$\text{Mean transit time} = -\frac{1}{jH(0)}\frac{\partial H(\omega)}{\partial \omega}\Big|_{\omega=0} \tag{4.14}$$

The partial derivative of $H(\omega)$ with respect to ω requires finding the partial derivative of the exponential term from equation 4.13:

$$\frac{\partial H(\omega)}{\partial \omega} = \frac{\partial\, e^{(x_1-x_0)\zeta(\omega)}}{\partial \omega} = \frac{-j}{2D}(x_1-x_0)\left(\frac{Q^2}{4D^2}+\frac{j\omega}{D}\right)^{-1/2} e^{(x_1-x_0)\zeta(\omega)} \tag{4.15}$$

The derivative of $H(\omega)$ at $\omega = 0$ is found as:

$$\frac{\partial H(\omega)}{\partial \omega}\Big|_{\omega=0} = \frac{\partial\, e^{(x_1-x_0)\zeta(\omega)}}{\partial \omega}\Big|_{\omega=0} = \frac{-j}{Q}(x_1-x_0)\, e^{(x_1-x_0)\zeta(0)} \tag{4.16}$$

which, when divided by $-jH(0)$ to give the mean transit time, becomes:

$$\text{Mean transit time} = \frac{(x_1 - x_0)}{Q} \qquad (4.17)$$

where $(x_1 - x_0)$ represents the vascular volume between the points x_0 and x_1.

This result shows that the transfer function, $H(\omega)$, which is produced using Fourier analysis of recorded tracer concentration transients can be used to calculate the mean transit time of the impulse response, and that this mean transit time is clearly related to parameters which have physiological significance in accordance with the convection-dispersion model of tracer transport. This result also justifies the use of the second Stewart-Hamilton equation in studies where the impulse response and its mean transit time were found by other means based on linear systems' analysis.

Branching of Vessels

Modifying the model to include the branching of vessels is not difficult. If the convection-dispersion model is assumed to be applicable to transport through all vessels in a network of B vessels, then the i^{th} branch would have its own associated transfer function, $H_i(\omega)$, with the point of its emergence from a bifurcation being analogous to the boundary x_0. The transfer function which represents transport through the entire network to the end of the B^{th} vessel, call it $H_B(\omega)$, is simply equal to the multiplication of all intermediate transfer functions:

$$H_B(\omega) = \prod_{i=1}^{B} H_i(\omega) \qquad (4.18)$$

Because the form of the transfer function is exponential, evaluation of equation 4.18 essentially involves only the summation of exponents:

$$H_B(\omega) = \exp\left[\sum_{i=1}^{B} \frac{V_i Q_i}{2D_i} - \left(\frac{V_i^2 Q_i^2}{4D_i^2} + \frac{j V_i^2}{D_i} \omega \right)^{1/2} \right] \qquad (4.19)$$

where V_i is used to represent the vascular volume of the i^{th} vessel. Using the same analysis presented in equations 4.14 - 4.17, the mean transit time through the network of branched vessels is found to be equal to the sum of the transit times through the intermediate vessels:

$$\text{Mean transit time} = \sum_{i=1}^{B} \frac{V_i}{Q_i} \qquad (4.20)$$

As can be seen from this expression, the reciprocal of the mean transit time is inversely proportional to the flow through the network of vessels. The exact relationship is a nonlinear, weighted average of the flow through the vasculature. It is precisely this reciprocal of the mean transit time which has been used previously to measure regional blood flow [Wolpers et al. 1984; Whiting et al. 1986; Carlsen & Hedegaard 1987] and was used in the present work as an index of perfusion. The mean transit time calculated with the X-ray fluorescence system refers to the mean time required for tracer to reach the region of interest in the myocardium from the left ventricular lumen.

Computation of Convection-Dispersion Parameters from Transfer Function Analysis

Another characteristic of tracer transport, namely tracer dispersion, can also be found using the transfer function. Although the value of this parameter was not used in the present study, its computation, as well as the mean transit time's, will be presented in this section.

Just as the first moment of the impulse response was shown to be proportional to flow rate, the second moment of the impulse response can be shown to be proportional to the effective diffusivity of the tracer's transport. The normalized second moment of the impulse response is equal to the second moment divided by the zeroeth moment and, again using the moment theorem, can be found from the transfer function with the following equation:

$$\text{Normalized second moment} = -\frac{1}{H_B(0)}\frac{\partial^2 H_B(\omega)}{\partial \omega^2}\Big|_{\omega=0} \qquad (4.21)$$

The transfer function $H_B(\omega)$, defined in equation 4.19, is used here to give a general result. Using the result of equation 4.15, the second derivative of $H_B(\omega)$ is found to be:

$$\frac{\partial^2 H_B(\omega)}{\partial \omega^2} = \left\{ \sum_{i=1}^{B} \frac{-V_i}{4D_i}\left(\frac{Q_i^2}{4D_i^2} + \frac{j\omega}{D_i} \right)^{3/2} + \right.$$

$$\left. + \left[\sum_{i=1}^{B} \frac{-jV_i}{2D_i} \left(\frac{Q_i^2}{4D_i^2} + \frac{j\omega}{D_i} \right)^{1/2} \right]^2 \right\} \exp\left[\sum_{i=1}^{B} V_i \zeta_i(\omega) \right] \qquad (4.22)$$

When equation 4.22 is evaluated at $\omega = 0$ and divided by $-H_B(0)$, the normalized second moment is found to be.

$$\text{Normalized second moment} = \sum_{i=1}^{B} \frac{2V_iD_i}{Q_i^3} + \left(\sum_{i=1}^{B} \frac{V_i}{Q_i} \right)^2 \qquad (4.23)$$

A more convenient parameter of dispersion is produced by subtracting the square of the mean transit time from the normalized second moment. The result is an expression known as the normalized second moment about the centroid:

$$\text{Normalized second moment about the centroid} = 2 \sum_{i=1}^{B} \frac{V_iD_i}{Q_i^3} \qquad (4.24)$$

As can be seen from equation 4.24, the normalized second moment about the centroid is directly related to the effective diffusion coefficients. Evaluation of the effective diffusion coefficients may be important for studies of flows through capillary beds where dispersion has been shown to be related to tracer diffusivity across capillary walls [Perl & Chinard 1968; Tepper et al. 1978].

The mean transit time and the normalized second moment can also be calculated from the transfer function without requiring the calculation of derivatives in frequency space. A more straightforward method for finding these values and other characteristics of tracer transport is based on the polynomial expansion of the transfer function and is presented below.

Consider the Maclaurin series expansion of $H_B(\omega)$, used here again to give a general result:

$$H_B(\omega) \approx 1 - j\omega \sum_{i=1}^{B} \frac{V_i}{Q_i} - \omega^2 \left[\sum_{i=1}^{B} \frac{2V_iD_i}{Q_i^3} + \left(\sum_{i=1}^{B} \frac{V_i}{Q_i} \right)^2 \right] +$$

$$+ j\omega^3 \left\{ \sum_{i=1}^{B} \frac{12V_iD_i^2}{Q_i^5} + \left(\sum_{i=1}^{B} \frac{V_i}{Q_i} \right) \left[\sum_{i=1}^{B} \frac{6V_iD_i}{Q_i^3} + \left(\sum_{i=1}^{B} \frac{V_i}{Q_i} \right)^2 \right] \right\} + \ldots \qquad (4.25)$$

Upon examination of equation 4.25, the moments of the impulse response can be found in the coefficients of their respectively ordered polynomial terms. The physiologically significant characteristics of an impulse response, and therefore of tracer transport, can be determined by fitting the above polynomial series to an experimentally produced transfer function near $\omega = 0$.

The expansion above is carried out only to the third order polynomial because it has been suggested that characteristics of an impulse response corresponding to greater than the third moment would probably not play an important role in characterizing biological flows [Bassingthwaighte & Ackerman 1967]. Nevertheless, if higher order moments were considered important, the transfer function developed here does allow for the interpretation of higher order moments of the impulse response for systems where tracer transport can be described with the convection-dispersion model.

Practical Application of Transfer Function Analysis to Physiologic Data

The application of a theoretically sound analysis technique is often hindered by problems associated with the production and recording of indicator-dilution curves, such as an inability to estimate actual tracer concentration, unavoidable signal noise, and the preparation of data for computer analysis. Through an example, the following section will illustrate practical aspects of the transfer function analysis technique as they apply to finding characteristics of an impulse response from recorded indicator-dilution curves.

Figure 4.2 shows a pair of indicator-dilution curves representing the X-ray induced fluorescence of an intravenously injected iodinated tracer as it passed through the left ventricular lumen and subsequently through a discrete region (~22 mm^3) of the myocardium in a canine. If the assumption is made that the tracer concentration in the left ventricular lumen is not appreciably different from that at the ostium to the coronary arteries, then the tracer transient in the left ventricle can be taken to represent the inlet function for a multiple branching system of coronary vessels.

Because the myocardial transient represents the fluorescence of tracer within a volume of 22 mm^3, this transient can not be considered that from only a single vessel. However, if the tracer is well mixed at the level of the inlet, thereby guaranteeing the distribution of tracer being proportionally equal to the distribution of flow, then the myocardial transient does represent

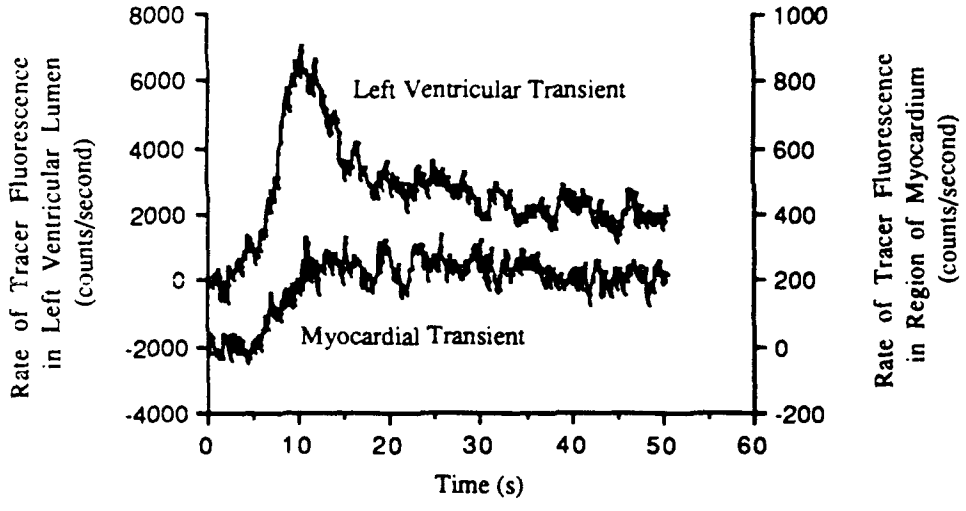

Figure 4.2: Sample Tracer Transients Subjected to Transfer Function Analysis. These indicator-dilution curves represent the X-ray fluorescence of the tracer recorded in the left ventricular lumen and in a region of the myocardium after a 10 cc bolus of Omnipaque®-350 (Winthrop-Breon Labs) was injected into the cephalic vein of a closed-chested dog.

the average transient for the vessels which occupy the region under observation. The myocardial transient can therefore be considered as the outlet function for the vasculature that perfuses the region of interest.

The curves in figure 4.2 are discrete functions of time and represent the tracer's rate of fluorescence sampled at intervals of 0.1 seconds. At relatively low tracer concentrations, the rate of fluorescence is linearly related to the actual tracer concentration. This is an important relation because, in many cases, the actual calibration constants which would relate fluorescence to tracer concentration may be unknown due to radiation attenuation by the thorax. In this example, it will be shown that only the knowledge of the linear relationship, not of the actual calibration constants themselves, is all that is required for effective transfer function analysis.

The first step in the transfer function analysis requires taking the discrete Fourier transform of each curve. The discrete Fourier transform, however, assumes the function to be periodic, and the curves must therefore be represented as periodic functions in such a way as not to alter the values of interest. This requirement has been addressed by Coulam et al. [1966] who used a Gaussian function "tail" to bring the steady state concentrations to baseline. Other windowing techniques are acceptable, such as the Hanning window which is based on a cosine function [Oppenheim & Shafer 1975]. In this example, a modification of the Hanning window was used to extend the transient and produce a smooth transition back to baseline at time 409.6 sec.

With the curves properly windowed, the discrete Fourier transforms of the indicator-dilution curves are found using the following definition:

$$C(\theta) = \sum_{n=0}^{N-1} c(n)\ e^{-j(2\pi/N)n\theta} \tag{4.26}$$

where c(n) = a discrete sequence representing a time function sampled at intervals of T seconds; n = a discrete time point (t = nT); N = the total number of data points which makes up a complete windowed curve (N = 4096); and θ = a discrete angular frequency point ($\omega = \frac{2\pi}{NT}\theta$) [Oppenheim & Shafer 1975]. The experimentally observed transfer function $H_{ex}(\theta)$ can then be defined as the discrete Fourier transform of the recorded myocardial transient, call it M(n), divided by the discrete Fourier transform of the recorded left ventricular transient, L(n):

$$H_{ex}(\theta) = \frac{M(\theta)}{L(\theta)} \tag{4.27}$$

The relationship between this experimentally found transfer function and the theoretical transfer function for the system must now be found.

The theoretical transfer function for a multi-branching system has already been defined in equation 4.19. Its discrete time representation, $H_B(\theta)$, calculated with inlet and outlet tracer concentration functions f(n) and g(n), respectively, is given as follows:

$$H_B(\theta) = \frac{G(\theta)}{F(\theta)} = \exp\left[\sum_{i=1}^{B} \frac{V_i Q_i}{2D_i} \cdot \left(\frac{V_i^2 Q_i^2}{4D_i^2} + \frac{j V_i^2}{D_i} \left(\frac{2\pi}{NT}\theta \right) \right)^{1/2} \right] \tag{4.28}$$

The left ventricular concentration transient representing the system's inlet function f(n) is equal to the recorded fluorescence transient L(n) multiplied by a linear calibration constant k_L, i.e. $f(n) = k_L L(n)$. The value of this calibration constant depends on some possibly unknown factors such as detection efficiency, irradiating X-ray beam attenuation and exiting photons' interactions with bone and tissue. The myocardial fluorescence transient would also require a calibration constant, k_M, to produce the system's outlet function, i.e. $g(n) = k_M M(n)$. After considering the relationship of the recorded curves L(n) and M(n) with the corresponding functions f(n) and g(n), the experimental transfer function defined in equation 4.27 is found to be related to the theoretical transfer function as follows:

$$H_{ex}(\theta) = \frac{k_L}{k_M} H_B(\theta) \tag{4.29}$$

Using a Maclaurin series expansion for $H_B(\theta)$ defined in equation 4.28, $H_{ex}(\theta)$ is taken to be equal to the following approximation near $\theta = 0$:

$$H_{ex}(\theta) \approx \frac{k_L}{k_M}\left(1 - j\left(\frac{2\pi}{NT}\theta\right)\sum_{i=1}^{B}\frac{V_i}{Q_i} - \left(\frac{2\pi}{NT}\theta\right)^2\left[\sum_{i=1}^{B}\frac{2V_iD_i}{Q_i^3} + \left(\sum_{i=1}^{B}\frac{V_i}{Q_i}\right)^2\right] + \right.$$

$$\left. + j\left(\frac{2\pi}{NT}\theta\right)^3\left\{\sum_{i=1}^{B}\frac{12V_iD_i^2}{Q_i^5} + \left(\sum_{i=1}^{B}\frac{V_i}{Q_i}\right)\left[\sum_{i=1}^{B}\frac{6V_iD_i}{Q_i^3} + \left(\sum_{i=1}^{B}\frac{V_i}{Q_i}\right)^2\right]\right\} + \ldots\right) \tag{4.30}$$

The coefficients of the above polynomial series are equal to the moments of the impulse response multiplied by a factor of $\frac{k_L}{k_M}\left(\frac{-j2\pi}{NT}\right)^i$, where i is the order of the moment. The characteristics of the impulse response can therefore be determined by fitting the real and imaginary parts of this series to their

respective portions of the experimentally produced transfer function $H_{ex}(\theta)$ near $\theta = 0$ using polynomial regression analysis.

Figure 4.3 shows the real (Re) and imaginary (Im) portions of $H_{ex}(\theta)$ at low frequencies. Each value of the functions $\mathrm{Re}H_{ex}(\theta)$ and $\mathrm{Im}H_{ex}(\theta)$ is reported as a distribution with a mean and standard deviation. These distributions are manifestations in the frequency domain of the noise in the experimental data. Each distribution was calculated by choosing a series of different, yet suitable, times for the transients' continuations with their Hanning "tails" before Fourier transformation.

The specific range of θ over which the polynomial regression is to be applied is dictated by the extent to which the regression is desired to represent the data near $\theta = 0$. If only the value for the mean transit time were required, it would be advantageous to select a range of θ which would not require the calculation of extraneous terms and would still provide a good representation of the data set for at least the first order term. For the present example, the range of $\theta \leq 9$ was found to be adequate to ensure a good representation of the linear term while not requiring the determination of too many unnecessary higher order terms.

Having chosen a range, polynomial regression analysis is initiated by establishing the order of the polynomial to be fit to the data. This is done using the step-up method where higher order orthogonal polynomials are applied to the residuals of the previous order fit until significant contributions are no

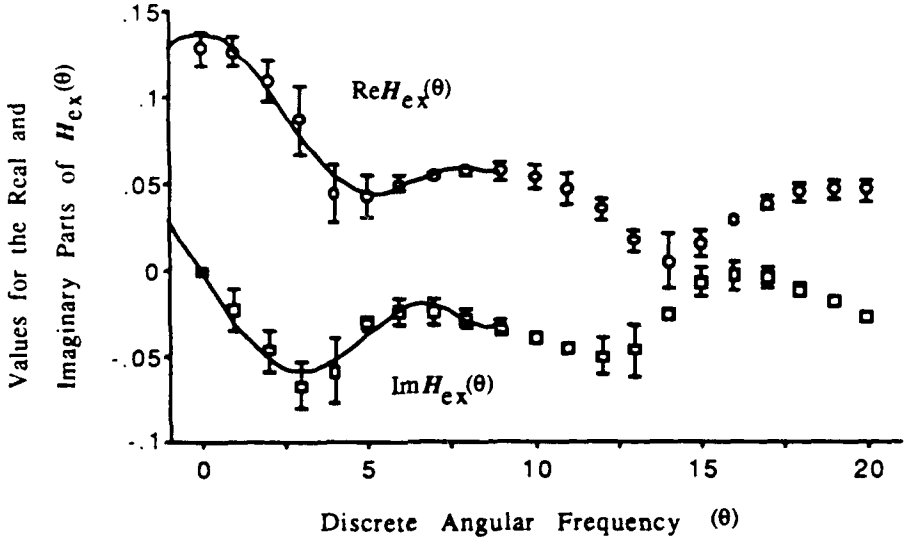

Figure 4.3: Transfer Function Found for Sample Transients. The real and imaginary parts of the example transfer function are shown as functions of theta, the discrete angular frequency which is expressed as integer values. Polynomial regression analysis was applied over the range of theta $\leq$ 9 after determining the fits to require an eighth order fit. The regression lines illustrate their ability to represent well the trend of the data near theta = 0.

longer acquired [Freund & Minton 1979]. Having determined the highest order polynomial to be fit to the data, polynomial regression analysis can then be applied using standard least squares methods.

For this example, the polynomial representation of the transfer function for $\theta \leq 9$ was found to require an eighth order polynomial expression whose first four terms are given below:

$$H_{ex}(\theta) = 0.1347 - 3.094\text{x}10^{-2}\, j\theta - 8.50\text{x}10^{-3}\, \theta^2 + 1.479\text{x}10^{-3}\, j\theta^3 + \ldots \qquad (4.31)$$

The computed regression lines are shown with the data on figure 4.3.

In order to find specific characteristics of tracer transport, recall that the i^{th} moment of the impulse response is equal to the coefficient of the i^{th} ordered term of equation 4.31 divided by $\frac{k_L}{k_M}\left(\frac{-j2\pi}{NT}\right)^i$. The mean transit time, defined as the first moment of the impulse response divided by its zeroeth moment, is then determined as follows based on the result of equation 4.31:

$$\text{Mean transit time} = \frac{-j\,0.03094}{k_L/k_M\left(\frac{-j2\pi}{NT}\right)} \Big/ \frac{0.1347}{k_L/k_M} = 14.9 \text{ sec.} \qquad (4.32)$$

Other characteristics of the impulse response can also be found from the coefficients of the polynomial representation of $H_{ex}(\theta)$ in a similar manner. It should be noted that the values of the calibration constants k_L and k_M or of their ratio are not necessary for these calculations.

The analysis method described in this section was used to analyze the data acquired from animal experiments performed in this work. The reciprocals of the calculated mean transit times were compared to myocardial blood perfusion measured by radioactive microspheres. Despite the linear correlation found from this comparison, which will be reported more thoroughly in Chapter 5, it is still quite reasonable to expect a nonlinear relationship between absolute perfusion and the reciprocal of the mean transit time through a multi-branching network. In recognition of this likely nonlinear relationship, the normalized second moment about the centroid has been used along with the mean transit time in a preliminary attempt to calculate regional myocardial perfusion strictly from these two parameters [Palmer & McInerney 1988]. These latter results, however, are not reported in this dissertation.

Chapter 5

MYOCARDIAL PERFUSION MEASUREMENTS

In order to demonstrate the use and effectiveness of the current X-ray fluorescence system, myocardial perfusion studies were performed in a canine model. The specific aim of these studies was to produce several different myocardial perfusion conditions, measure regional myocardial perfusion using the fluorescence system and a recognized standard, namely radioactive microspheres, and compare the results obtained from each method. Evaluation of the efficacy of the X-ray fluorescence system in determining regional myocaridal perfusion was then based on the results of these studies.

This chapter presents first the methods used to produce various perfusion conditions in canines and the specific techniques with which regional myocardial perfusion was measured. Animal preparation and experimental procedure are then described detailing the use of the X-ray fluorescence system *in vivo*. Results are reported from two types of analyses: 1) the straightforward comparison of the reciprocals of the mean transit times as measured by X-ray fluorescence with the regional perfusion measured by radioactive microspheres, and 2) the comparison of the relative change in the reciprocals of mean transit times with the relative change in measured perfusion, both of which quantitated as the percent change of measured values during modifed perfusion states relative to the control condition in the same animal.

Materials and Methods

Thirteen mongrel dogs weighing within the range of 12-17 kg were used as subjects in this investigation of regional myocardial perfusion. Although the coronary anatomy of canines is slightly different from that of humans, the most notable differences being the hearts' sizes and the relative abundance of colateral vessels in the canine heart, a canine model was considered anatomically appropriate. The acceptance by the scientific community of the canine as a suitable model for perfusion experiments and the availability of the animals at The Milton S. Hershey Medical Center also contributed to the choice of this model for the myocardial perfusion studies reported here.

Hemodynamic Interventions

In these studies, it was necessary to produce various perfusion conditions in the subjects. In order to produce low myocardial perfusion conditions, simple ligation of coronary arteries was performed. For an increase in myocardial perfusion, an intravenous infusion of adenosine (SIGMA Chemical Co., St. Louis, MO) was used. Adenosine is a powerful vasodilator and has been hypothesized as the specific biochemical mechanism responsible for increasing coronary flow during periods of increased demand for blood [Rubio & Berne 1975]. Reasonable infusion rates of adenosine which increase myocardial perfusion in canines under experimental conditions have been well documented by previous investigators [Rumberger et al. 1987;

Wolfkiel et al. 1987] and were used as a guide to set the range of infusion rates in this investigation to be 0.1 - 1.0 mg/min-kg.

Perfusion Measurements by Radioactive Microspheres

The perfusion studies reported here required the measurement of regional myocardial perfusion by a technique which is recognized as a standard for measuring this quantity. The technique based on radioactive microspheres has been suggested to be such a technique [Heymann et al. 1977] and has been accepted as the "gold standard" for blood flow studies based on its ability to accurately measure perfusion, as demonstrated recently by Bassingthwaighte et al. [1987]. The method is based on the theory that the fraction of microspheres delivered to a region of tissue is equal to that fraction of the cardiac output which perfuses the region, assuming the microspheres were originally well mixed in the left ventricular blood pool. This latter requirement necessitates the injection of microspheres into the left atrium.

Spheres having a diameter greater than 10 μm are usually used to insure that they are trapped in the capillaries of a region which can be dissected and then analyzed for its specific radioactivity. The calculation of the actual blood flow to the region of interest requires knowing the amount of flow which can be attributed to the specific radioactivity of the tissue. This requirement is met by withdrawing blood from a major artery at a known rate. The specific activity of the withdrawn blood represents the withdrawal rate, and regional perfusion (RP) of the dissected tissue sample is therefore

calculated as follows:

$$RP = \frac{\text{tissue activity}}{\text{tissue mass}} \times \frac{\text{blood withdrawal rate}}{\text{blood sample activity}} \qquad (5.1)$$

and is reported in units of blood flow per tissue mass.

Other details which are mandatory for achieving accurate perfusion measurements with radioactive microspheres have been itemized by Heymann et al. [1977]. In the interest of depositing a sufficient number of microspheres for accurate radiation analysis, it was suggested that at least 400 microspheres per tissue sample be provided [Buckberg et al. 1971]. Because the amount of tissue dissected for myocardial perfusion measurements was on the order of 1 gram, the injection of 3×10^6 microspheres (4×10^5 microspheres/kg $\times \sim 7$ kg soft tissue weight available for perfusion after preparation [Wolfkiel et al. 1987]) was considered adequate to meet this stipulation. To further insure the well mixed criterion of the microspheres, ultrasonic disaggregation immediately prior to injection was recommended; three minutes of ultrasonic diaggregation in an ultrasonic bath were executed in these studies. And lastly, the withdrawal of blood at a rate comparable to the flow expected in a tissue sample, about 1 ml/min for 1 gram, was suggested; this requirement was met by withdrawing arterial blood at a rate of 2.91 ml/min with a withdrawal pump (Harvard Apparatus Co., Millis, MA).

The specific radioactive microspheres used in this investigation were purchased from the Nuclear Products Division of the 3M Co. (St. Paul, MN).

These microspheres, which were made of polystyrene, had diameters of 15 ± 3 μm to insure capture by capillaries and were stored in normal saline with 0.05% Tween-80® (Union Carbide), a solution which reduces the aggregation of microspheres. Four different radioisotopes (^{46}Sc, ^{95}Nb, ^{85}Sr, ^{141}Ce) were used in the flow studies although not all four were always available for each subject. Therefore, original plans calling for four or occasionally three flow studies per subject allowed for a total of 49 possible studies.

X-ray Fluorescence Measurements

The details of the X-ray induced fluorescence technique used in this series of perfusion studies have been described in the preceding chapters of this dissertation. An early version of the X-ray fluorescence system has been shown to be effective in determining the reciprocals of mean transit times which correlated highly (r = 0.92) with actual flows in a phantom model [Palmer et al. 1987]. These results encouraged the further development of this system for use *in vivo*.

It should be emphasized, however, that the X-ray fluorescence system utilized in these *in vivo* studies was still a prototype system and was not designed to address some of the problems associated with its possible application to humans. For example, the problem of attenuation by the thorax of the primary beam and of the emitted fluorescent X-rays had not yet been considered thoroughly and was therefore eliminated in the ***in vivo*** perfusion studies by removing the relevent portions of the thorax during animal

preparation. Careful consideration of the effects of attenuation would certainly be the next action to be undertaken after the efficacy of the X-ray fluorescence system was determined in this "open-chested" preparation.

In the studies reported here, an iodinated radiographic contrast agent was used as the flow tracer monitored by X-ray fluorescence. The specific contrast agent is a solution of diatrizoate meglumine and diatrizoate sodium, an ionic and hyperosmotic material which is known to acutely increase coronary blood flow during intracoronary injections [Bettmann & Morris 1986]. However, a significant diminishing of these reactions can be accomplished with an intravenous injection [Higgins et al. 1982]. In fact, flow studies performed by Lipton [1985] and Whiting et al. [1986] have shown that intravenously injected, ionic contrast agents were effective as flow tracers for studies of myocardial perfusion. Therefore, based on these findings, the contrast agents Hypaque®-76 (Squibb Pharmaceutical Co., Princeton, NJ) and Angiovist®-370 (Berlex Labs, Wayne, NJ), both of which containing 660 mg/ml diatrizoate meglumine and 100 mg/ml diatrizoate sodium, were considered satisfactory flow tracers. The amount of tracer injected for each study was 0.5 cc/kg, a reported maximum which can be injected without causing unacceptable reactive hyperemia [Higgins et al. 1982].

Animal Preparation

Each animal was anesthetized with sodium-pentobarbital (40 mg/kg) and supplimental doses were administered to maintain anesthesia. A mechanical respirator was used throughout the procedure to maintain a rate of 12 breaths per minute at 40% oxygen. Each dog underwent an acute thorocatomy exposing the heart completely. The pericardial sac was dissected and tacked to existing portions of the rib cage in order to cradle the heart and minimize excessive motion. This preparation permitted visual identification of the region of interest in the myocardium and eliminated the attenuation of the fluorescence signal due to the chest wall.

In addition, a femoral artery was cannulated for the positioning of a catheter in the descending aorta permitting the arterial blood withdrawal required for microsphere analysis. A femoral vein was also cannulated in those dogs which were to recieve an intravenous infusion of adenosine. A two inch angiocatheter was placed in the left jugular vein for the injection of iodinated flow tracer, and the left atrial appendage was cannulated for the injection of the radioactive microspheres.

To produce differential flows, six dogs underwent ligations of prominent coronary arteries supplying the region of the interest in the myocardium after two control studies. The other seven dogs were infused with adenosine after one control study. Adenosine infusions began 10 minutes before the start of each study and continued throughout the course of each study.

Procedure

Before each perfusion study, the X-ray beam was aimed at a portion of the left lateral wall of the left ventricle, approximately half way between the apex and base of the heart. Positioning the Ge detector's sensitive volume within the myocardium was achieved by translating the detector along the beam until X-ray photons scattered from the epicardial surface could be recorded, a procedure described by McInerney et al. [1987]. Using the epicardial surface as a reference point, the detector was then moved medially until the modulation of the scatter signal due to the beating heart could no longer be detected. The NaI detector's sensitive volume was positioned in the left ventricular lumen, a distance empirically determined to be 29 mm from the epicardial surface and which also agrees with the findings of Farmer et al. [1985].

Actual perfusion measurements began with the withdrawal of arterial blood. Then, with the dog's breath held in expiration, a bolus of tracer was injected into the jugular vein. Within 10-20 seconds after tracer injection, radioactive microspheres were injected into the left atrial appendage with a 10 cc saline flush. The frequency of K_α emissions from each sensitive volume was recorded by the X-ray fluorescence system. Each study required nearly 90 seconds to accumulate the tracer transients.

After performing all flow studies planned for each dog, the animal subject was euthanized with an overdose of pentobarbital. A transmural

section of the irradiated myocardium was dissected for measurement of myocardial perfusion by radioactive microspheres. A transmural sample was analyzed because it was assumed that the transmural iodine concentration was recorded due to the continuous motion of the beating heart relative to the Ge detector's stationary sensitive volume. The arterial blood samples and the tissue sample were counted for equal time periods in a gamma-counter (Packard model 5230) to determine the specific activities of their radioactive constituents. Regional perfusion for each study was then calculated using equation 5.1.

The recorded tracer transients were transferred to a mainframe computer (DEC VAX 11/780) for off-line analysis. The calculation of the mean transit times for the tracer to reach the region of interest from the left ventricular lumen were performed using the transfer function analysis technique described in Chapter 4.

Results

Of the 49 planned flow studies, 38 were performed successfully. Criteria for an unsuccessful study were death due to severe degradation of cardiac function after coronary ligations (n=3), difficulty in obtaining arterial blood samples (n=2), technical difficulties associated with maintaining a stable X-ray beam intensity (n=3), and positioning problems where both detectors were monitoring the left ventricular lumen or the Ge detector was monitoring a coronary artery (n=3).

Acquired fluorescence data typical of a successful study are shown in figure 5.1 where the iodine transient of the left ventricular blood pool is shown to have the characteristic shape, including the recirculation peak, reported by other groups [Whiting et al. 1986; Rumberger et al. 1987; Wolfkiel et al. 1987]. The shape of the iodine transient in the myocardium is also consistent with the findings reported by these groups.

The open-chested preparation eliminated most significant contributors to radiation attenuation and therefore facilitated the estimation of actual iodine concentration. Figure 5.2 shows the transients of figure 5.1 subjected to a smoothing algorithm and reported in units of iodine concentration. Estimates of iodine concentration in the left ventricular blood pool were corrected for the attentuation of the fluorescent photons due to 3 cm of tissue between the sensitive volume and the detector. Using this correction, the concentration of iodine in the left ventricular blood pool was calculated to achieve a maximum of ~9 mg/ml and eventually reach a steady state of ~1 mg/ml.

Estimates of iodine concentration in the myocardium were assumed not to require correction due to attenuation. Iodine accumulation in the myocardium was therefore found to reach a concentration of ~0.8 mg/ml. These calibrated curves of figure 5.2 demonstrate that the system was capable of monitoring very low concentrations of iodine and that these concentrations were within the linear range of the fluorescence - concentration relationship which was required for valid calculations of the mean transit time using transfer function analysis.

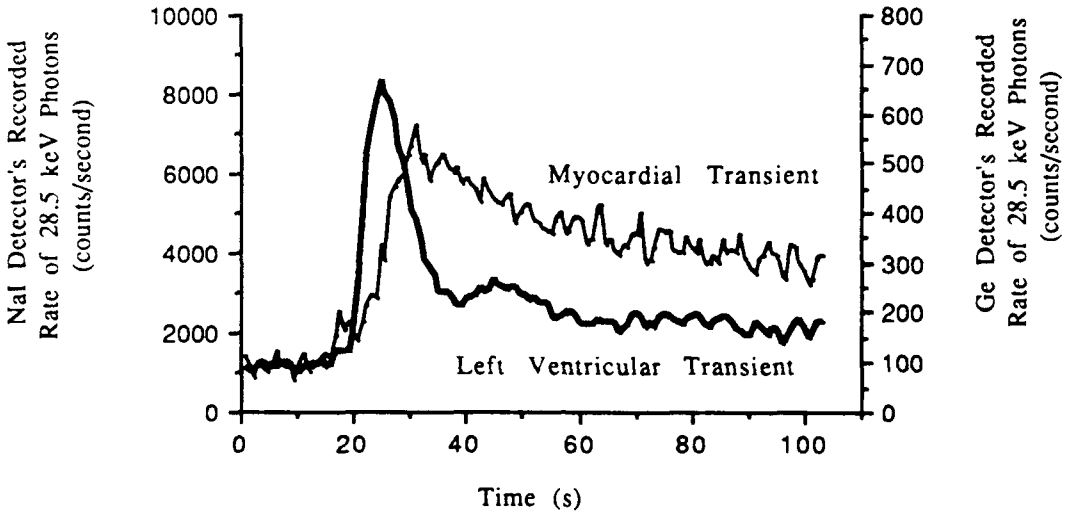

Figure 5.1: Typical Fluorescence Transients Recorded from the Left Ventricular Lumen and a Region of Interest in the Myocardium. These raw data represent the detected rate of 28.5 keV photons after an intravenous injection of iodinated tracer at time = 15 s.

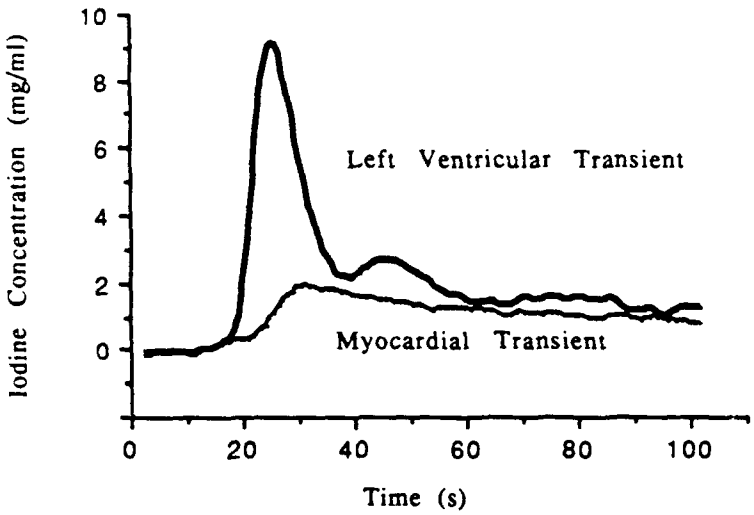

Figure 5.2: Typical Transients Smoothed and Calibrated. Iodine concentration is reported in units of mg/ml.

Table 5.1 lists the results of the perfusion studies. Each dog, intervention and result are listed for all 49 planned perfusion studies. Those studies which were not considered successful and therefore discounted in the final analysis are noted. Regional myocardial perfusion measured by radioactive microspheres is reported in units of milliliters per minute of blood flow per gram of tissue. The reciprocal of the mean transit time is reported in units of reciprocal seconds. The relative change of these values due to an intervention as compared to the first control study are reported in units of percent change. From table 5.1, it can be seen that the adenosine infusions for dogs numbered 10 and 11 resulted in a decrease in myocardial perfusion. This was due to infusion rates which were high enough to dramatically decrease arterial pressure in these subjects and subsequently diminish coronary blood flow.

Figure 5.3 shows the reciprocal of the mean transit times (MTT^{-1}) plotted against the perfusion (Q) measured by the radioactive microspheres. Linear regression analysis produced a correlation coefficient of $r = 0.71$. The regression line is represented by the equation, $MTT^{-1} = 0.0329\ Q + 0.0694$. The standard deviation of the residuals about the regression line are $\sim 0.0344\ sec^{-1}$, which shows that any one estimate of perfusion from the reciprocal of a mean transit time will have a standard deviation of $0.0344/0.0329 = \sim 1.05$ ml/min-g.

The comparison between relative change in perfusion (dQ) and relative change in the reciprocal of mean transit times ($dMTT^{-1}$) is shown in figure 5.4. Relative change is reported here as the percent change in a value from the first control flow study for each dog; consequently, only 25 data points are

available for comparison. Linear regression analysis shows a strong correlation, r = 0.88, for the regression line: $dMTT^{-1} = 0.459\ dQ - 10.7$. The standard deviation of the residuals from the regression line has a value of ~25.7% for $dMTT^{-1}$, which corresponds to a standard deviation of 25.7/0.459 = ~56.0% for any estimate of relative change in perfusion inferred from a relative change in the reciprocal of the mean transit time.

Table 5.1: Results of Canine Myocardial Perfusion Studies. Perfusion measurements (Q), the reciprocals of the mean transit times (MTT^{-1}), and their percent changes from control (dQ and $dMTT^{-1}$) are listed. Interventions are noted, as are the unsuccessful studies designated as follows: † = subject died after coronary ligations, * = problems arose while obtaining blood sample, $ = transients were indistinguishable, # = X-ray beam intensity was unstable.

	Dog #	Run #/Notes	Q (ml/min-g)	MTT^{-1} (s^{-1})	dQ (%)	$dMTT^{-1}$ (%)
1	1	1 / control	0.418	0.1517		
2		2 / †				
3		3 / †				
4		4 / †				
5	2	1 / *				
6		2 / control	0.416	0.1208		
7		3 / $				
8		4 / ligation	0.348	0.0746	-16.3	-38.0
9	3	1 / $				
10		2 / *				
11		3 / control	0.310	0.0639		
12		4 / ligation	0.348	0.0707	12.3	10.9

Table 5.1, continued:

	Dog #	Run #/Notes	Q (ml/min-g)	MTT^{-1} (s^{-1})	dQ (%)	$dMTT^{-1}$ (%)
13	4	1 / control	0.492	0.0778		
14		2 / control	0.806	0.0870	63.8	11.5
15		3 / ligation	0.406	0.0696	-17.5	-10.3
16		4 / ligation	0.140	0.0553	-71.5	-29.5
17	5	1 / control	0.928	0.0968		
18		2 / control	1.020	0.0780	9.9	-19.6
19		3 / ligation	0.541	0.0826	-41.7	-14.4
20		4 / ligation	0.640	0.0857	-31	-11.3
21	6	1 / control	0.669	0.0705		
22		2 / control	0.611	0.0731	-8.7	2.8
23		3 / ligation	0.713	0.0589	6.6	16.9
24		4 / ligation	1.500	0.1678	124.2	136.6
25	7	1 / control	1.350	0.1004		
26		2 / adenosine	2.820	0.1335	108.9	34
27		3 / adenosine	3.150	0.1484	133.3	48
28		4 / adenosine	2.220	0.0939	64.4	-6
29	8	1 / control	0.725	0.1153		
30		2 / adenosine	0.667	0.0912	-8	-20.9
31		3 / adenosine	3.250	0.2755	348.3	139.1
32		4 / adenosine	2.240	0.2262	209	96.5
33	9	1 / control	0.480	0.1045		
34		2 / #				
35		3 / #				
36		4 / $				
37	10	1 / control	0.504	0.1220		
38		2 / adenosine	0.096	0.0264	-81	-78.7
39		3 / adenosine	0.260	0.0453	-48.4	-63.1
40	11	1 / #				
41		2 / control	0.768	0.1420		
42		3 / adenosine	0.753	0.0797	-20	-43.7
43		4 / adenosine	0.458	0.1172	-40.4	-17.6
44	12	1 / control	0.472	0.0722		
45		2 / adenosine	0.487	0.0928	3.2	29.2
46		3 / adenosine	0.876	0.0917	85.6	27.8
47	13	1 / control	1.305	0.1010		
48		2 / adenosine	2.327	0.1086	78.3	7.9
49		3 / adenosine	5.041	0.1969	286.3	95

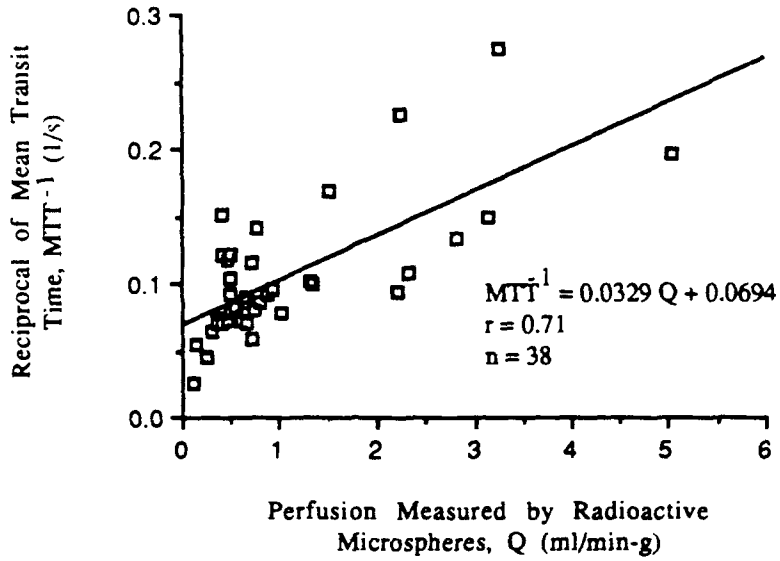

Figure 5.3: Comparison of the Reciprocal of the Mean Transit Time with Perfusion Measured by Radioactive Microspheres.

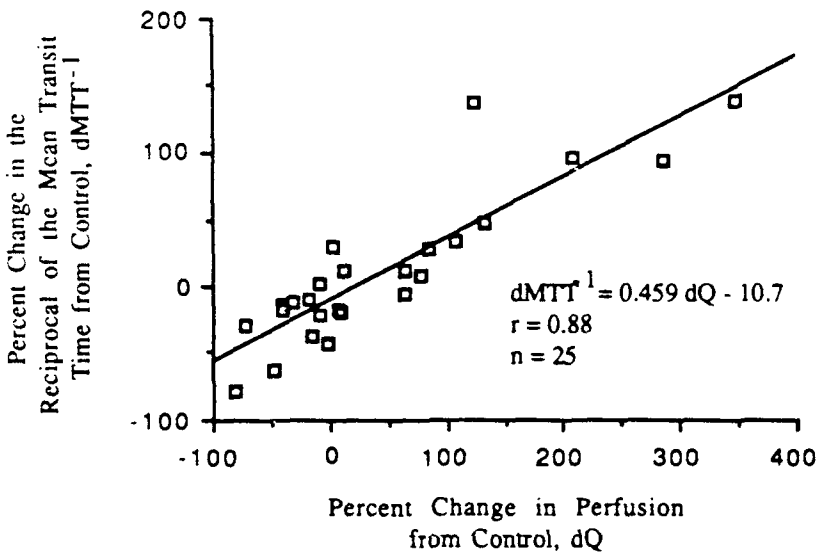

Figure 5.4: Comparison of the Percent Change in the Reciprocal of the Mean Transit Time with the Percent Change in Perfusion.

Discussion

The results of the *in vivo* perfusion measurement experiments can be summarized as follows: 1) the present X-ray fluorescence system does provide an acceptable means for monitoring iodine concentration as low as 1 mg/ml in very discrete regions, ~22 mm^3, of an intact heart; 2) the reciprocal of the mean transit time calculated using this method provides a measure of absolute perfusion with a standard deviation of 1.05 ml/min-g; as well as 3) a measure of the relative change in perfusion with a standard deviation of 56% change.

As mentioned earlier, the fundamental characteristics of the tracer transients recorded during these studies corresponded well to those anticipated based on reports by others [Whiting et al. 1986; Rumberger et al. 1987; Wolfkiel et al. 1987]. In addition, as shown most clearly in figure 5.1, there appears to be a small amount of fluorescence recorded in the myocardium transient immediately after tracer injection and before the tracer was recorded in the left ventricular lumen. This phenomenon was observed in approximately 30% of the recorded myocardial transients and may be due to a brief retrograde diffusion of tracer from the vena cava into the myocardium through the coronary sinus. It must be noted, however, that no data in the literature can be found to support this specific hypothesis. Despite the lack of an explanation, the brief fluorescence peak recorded in the myocardium was not considered to be a significant artifact, and the mean transit times were calculated without any adjustment of the original data.

In reference to the accuracy with which perfusion could be determined using this method, the minimal detectable difference is often reported and is defined as three times the standard deviation. Therefore, the minimal detectable difference for detecting absolute perfusion is ~3.15 ml/min-g, and the minimal detectable difference for relative perfusion is a 168% change in perfusion. Based on these results, the use of the present X-ray fluorescence system for clinical work or for research would be considered unacceptable for measuring absolute regional myocardial perfusion. The wide range of perfusion states to which one measurement may correspond does not make this prototype system attractive for investigations which usually require measurements to be accurate to within ± 0.5 ml/min-g. The use of this system for measuring relative perfusion, however, may be viable.

Measurements of relative increases in flow may be accurate enough to satisfy some needs. Normal coronary reserve in humans has been shown to be represented by increases in coronary flow on the order of 300 - 500% [Marcus et al. 1987]. Because the present system was found to be able to determine coronary reserve to within a 170% change in perfusion, this technique may be a viable means for distinguishing between normal and diminished coronary reserve. However, it must be recognized that, because severely under perfused regions of the heart may still elicit normal values for coronary reserve, the real utility of this system would be in evaluating those regions of the myocardium which have already been identified as having normal resting flows but may be at risk during periods of increased demand for blood supply.

In addition to the results mentioned above, there are some other notable characteristics of the results which must be addressed. For example, an obvious characteristic of the regression line shown in figure 5.3 is the substantial offset found along the ordinate. This offset would indicate that the tracer can be expected to eventually perfuse a region where microspheres would indicate no flow, as would be the case with an infarct. Studies performed by others have shown that the flow tracer used here does indeed diffuse through interstitial space to reach infarcted regions of the myocardium [Higgins et al. 1979; Doherty et al. 1981]. Their results show that a mean transit time to infarcted regions would be on the order of 60-120 seconds, whose reciprocals range in ~0.016-0.008 sec^{-1}. However, the offset observed in figure 5.3 is 0.694 sec^{-1} and is significantly greater than the 0.016 sec^{-1} that might be expected with diffusion transport. Therefore, the offset observed in figure 5.3 is probably only partially due to diffusion transport.

Another interesting aspect of the results presented in figure 5.3 concerns its prediction of the vascular volume of the coronary tree. Previous work by others has shown that the reciprocal of a tracer's mean transit time through a conduit correlates linearly with the actual flow through that conduit [Meier & Zierler 1954; Spalding 1958]. The slope of this relationship is equal to the reciprocal of the volume through which the tracer must pass. If the coronary vasculature were considered as a single conduit, then the slope shown in figure 5.3 would correspond to a volume of ~30 cc. Although this may be a reasonable approximation of the volume between the left ventricular lumen and the myocardium, it should be noted that most of the mean transit

time is associated with transport through the coronary vessels. A volume of ~30 cc for a coronary tree is much greater than the maximum volume of 2 cc predicted by the coronary casts of canines made by Levesque and Nerem [1983].

Negotiating the troublesome issues surrounding the offset and the slope of the relationship between the reciprocal of the mean transit time and regional perfusion may simply require that this relationship be nonlinear. A model of tracer transport which predicts a nonlinear relationship has already been developed in Chapter 4; it is the contribution of the branching of vessels which must now be examined. Consider a single bifurcation like that shown in figure 5.5. According to the result of equation 4.19, the mean transit time for a tracer to pass from the origin of the parent vessel to the end of the daughter vessel is given as:

$$\text{Mean transit time} = \frac{V_p}{Q_p} + \frac{V_d}{Q_d} \tag{5.2}$$

where V_p and V_d are the volumes of the parent and daughter vessels, respectively, and Q_p and Q_d are their flow rates. The reciprocal of the mean transit time is then found to be a nonlinear function of Q_d, the flow of interest:

$$MTT^{-1} = \left(\frac{V_p}{Q_p} + \frac{V_d}{Q_d}\right)^{-1} = \frac{Q_d}{V_d + Q_d \frac{V_p}{Q_p}} \tag{5.3}$$

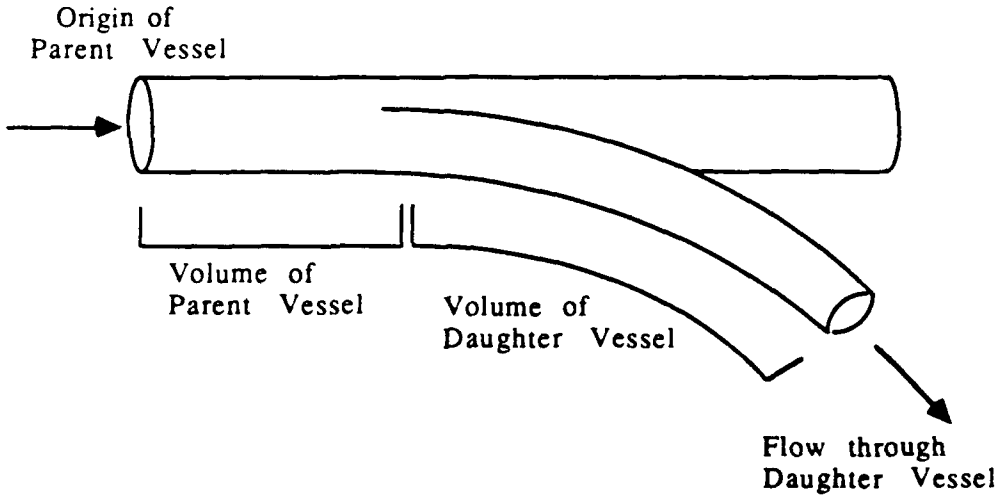

Figure 5.5: Schematic of a Single Bifurcation. This figure is useful for illustrating the nonlinear relationship between the daughter vessel's flow rate and the reciprocal of the mean transit time for a tracer to reach the tissue supplied by the daughter.

Linear regression applied to data that follow this relationship will produce varying slopes and offsets depending on the range of flows investigated. As figure 5.6 depicts, the regression line at relatively low daughter flows would have a steep slope and little offset. For relatively higher daughter flows, the slope would not be as steep and the offset along the ordinate would be substantial. If the branching of vessels were a reasonable explanation to the results shown in this study, the flows investigated here were high enough to elicit a significant offset and a diminished slope.

Another piece of evidence which points toward the possibility of a multibranching system can be found in the dMTT vs. dQ relationship shown in figure 5.4. If the single conduit model were sufficient, the slope of this relationship would be unity; however, a slope of less than half of unity is found. This could be a result of vessel branching where, even if flow through a daughter branch were doubled and the mean transit time through the daughter were then proportionately altered, the total mean transit time through both parent and daughter vessels would change in less proportion to the change in flow through the daughter.

Based on the observations made above, more accurate estimates of myocardial perfusion from the indicator-dilution method used here would probably require a model of tracer transport through the coronary vasculature which accounts for influences made by the branching of vessels.

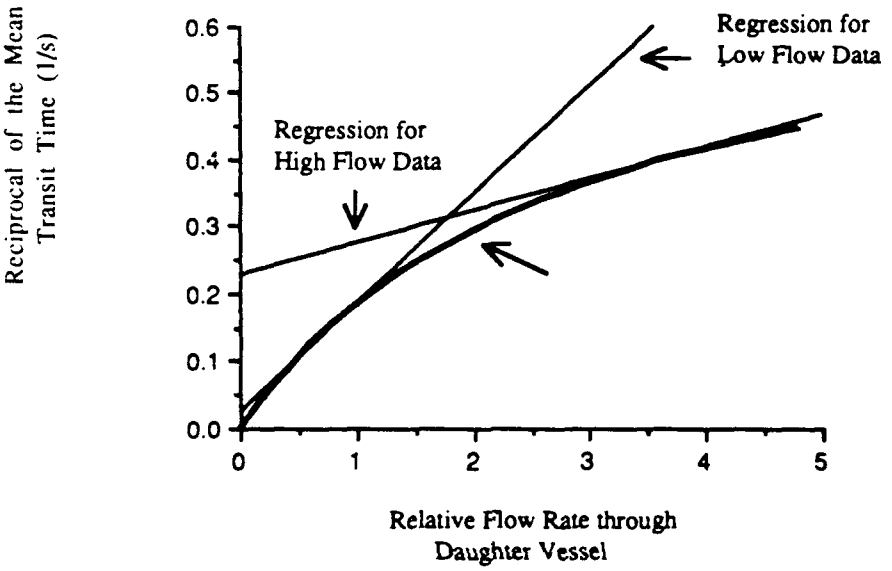

Figure 5.6: Nonlinear Relationship between the Reciprocal of the Mean Transit Time and the Flow through a Distal Branch of a Bifurcation. Linear regression applied to data when daughter flow is very low will produce little offset and a slope which approaches a value equal to the reciprocal of the volume of the daughter branch. Linear regression applied when daughter flow is a high percentage of the parent's flow will produce a greater offset and a diminished slope.

Chapter 6

SUMMARY AND CONCLUSION

This dissertation has strived to demonstrate that an X-ray induced fluorescence system can be used to measure regional myocardial perfusion. The specific goals of the work reported here were to develop a prototype system, to model tracer transport through the coronary circulation, to demonstrate and verify the use of the system *in vivo*, and to judge its overall efficacy for possible future development. Although the system's development and trial have been reported in detail, a qualitative evaluation of this system's performance has not yet been given. It is the intention of this chapter to bring together the major points demonstrated in each of the preceding chapters and then to evaluate the effectiveness of X-ray induced fluorescence in determining regional myocardial perfusion.

Summary

There was only one specific purpose of the X-ray fluorescence system developed in this work: to monitor accurately iodine concentration transients which arise in an intact heart. Based on the indicator-dilution curves presented in figure 5.1, it is justified to conclude that X-ray induced fluorescence does provide good recordings of iodine concentration transients in an intact heart of an open-chested dog. In quantitative terms, the signal-to-noise ratio at an iodine concentration of 1 mg/ml for the present system's Ge detector operating with an open-chested subject is SNR(1) = 11.7, as reported in

figure 3.3. This measure of system performance can be used as a reference when comparing future uses and developments of this technique.

The model of tracer transport presented in Chapter 4 is one which shows perfusion to be quantitatively represented by characteristics of tracer transport. The calculation of these characteristics, including the mean transit time, is readily accomplished with the use of transfer function analysis. Although only the mean transit time was used in the present work, the incorporation of other transport parameters, such as the normalized second moment, may be helpful in the future. Furthermore, the influence of the branching of coronary vessels on these transport parameters may have to be more carefully considered in order to create a more realistic model of tracer transport.

The results of the *in vivo* perfusion measurement experiments provided the first indication that the X-ray induced fluorescence system developed here is an effective tool for monitoring iodine concentration transients in open-chested animals. The determination of absolute perfusion through the use of the reciprocal of the mean transit time was found not to be particulary accurate. However, the system was shown to provide a reasonably accurate indicator of relative change in perfusion due to some intervention. This capability may be useful for determining a clinically important parameter, namely coronary flow reserve.

The need for determining coronary flow reserve noninvasively and in very discrete regions of the myocardium makes this technique appealing. However, before an X-ray fluorescence system can be considered for clinical use, or even for research purposes, the efficacy of the system in closed-chested preparations must first be investigated.

Future Use and Development

The further development of the present system would be dictated by the specific needs of clinical and research studies. The most obvious requirement is the ability to measure perfusion in a closed-chested preparation. The single detail of the closed-chested preparation which must be more thoroughly considered is the attenuation of the incident beam and of the fluorescence photons due to an intact thorax. Another need prescribed by potential users of this system is the monitoring of discrete regions within the transmural section of the myocardium. Due to the natural periodic motion of the beating heart, monitoring precisely these discrete regions of the myocardium would require counting photons only during selected periods of the cardiac cycle.

Attenuation poses two problems: first is the inability to calculate absolute concentrations of iodine, and second is the decrease in signal-to-noise ratio. The lack of absolute iodine concentration measurements is not a great problem, considering that the model of tracer transport requires only a linear relationship between fluorescence and iodine concentration. However, the issue of signal degradation is a significant one.

If the present system were used in a closed-chested subject, the fluorescence signal as well as the background radiation would be cut dramatically. Based on the calculated attenuation of 28.5 keV photons through 6 cm of soft tissue [Hubbell 1969], both detectors' signals would be reduced to ~0.05 of their open-chested counterpart. For the Ge detector, the signal-to-noise ratio of the closed-chested preparation would be:

$$SNR_{closed}(1) = SNR_{open}(1) \times \sqrt{0.05} \approx 2.62 \qquad (6.1)$$

where $SNR_{open}(1) = 11.7$ as mentioned above.

In order to restore the signal-to-noise ratio to a value comparable to the open-chested value, three modifications to the present system can be made: 1) increase the sensitive volume of the Ge detector, 2) increase the solid angle subtended by the Ge detector, or 3) increase the intensity of the incident X-ray beam. Any combination of these modifications is possible as long as there is a 20-fold increase in the signal. The factor 16 is required because $\sqrt{20} \approx 4.5$, the factor which would restore the $SNR_{closed}(1)$ to $SNR_{open}(1)$.

Before suggesting a specific modification, the issue of gating to the cardiac cycle should also be addressed. Gating the system's counting to the portion of the cardiac cycle where motion is at a minimum would restrict counting during diastole which lasts about one half of the cardiac cycle [McInerney 1989]. Therefore, the signal-to-noise ratio would be further reduced by the factor $\sqrt{0.5}$:

$$SNR_{closed+gated}(1) = SNR_{open}(1) \times \sqrt{0.05} \times \sqrt{0.5} \approx 1.85 \qquad (6.2)$$

Based on the above results, a gated system would have to provide ~40 times more fluorescence if it were to be used in a closed-chested preparation and still provide an equivalent signal-to-noise ratio achieved with the present system on an open-chested preparation. In order to regain this signal-to-noise ratio, an increase in sensitive volume by 20 fold can be tolerated, in fact a 40 fold increase to 1 cc would still be quite acceptable. Increasing the solid angle subtended by the Ge detector would also be acceptable and can be accomplished in two ways, by positioning the detector closer to the subject or by increasing the crystal area. Increasing crystal area can be done by using a larger detector or by incorporating another detector to monitor the same region. In addition, the beam's intensity can easily be doubled, particulary if it were also gated to irradiate only during periods of counting. Radiation dose would therefore not be significantly increased in this case with the irradiating beam is gated to the cardiac cycle.

Conclusion

The results of the studies reported in this dissertation do encourage the further development of an X-ray fluorescence system which can be used to measure regional myocardial perfusion in the closed-chested situation. Modifications of the present system, as suggested above, can be tolerated in order to provide tracer transients with the necessary signal-to-noise ratios for accurate analyses. Although the measurement of absolute perfusion was not

demonstrated here, a reasonably accurate determination of the percent change in perfusion due to an intervention was provided by the reciprocal of the mean transit time. It should be noted, however, that the reciprocal of the mean transit time alone is probably not an optimal index of myocardial perfusion due to their nonlinear relationship. In the future, consideration should be given to the many different methods for analyzing tracer transients similar to those recorded with X-ray fluorescence, including the incorporation of the second moment of the impulse response which was shown to be at least promising in providing values for absolute perfusion [Palmer & McInerney 1988]. When these concerns have been addressed, the attributes which make X-ray fluorescence an attractive technique would continue to be offered in the closed-chested situation: good spatial resolution, quantitative determination of flow parameters, noninvasive properties including no catheterization and low radiation dose, and relatively low cost.

BIBLIOGRAPHY

Aris, R. On the dispersion of a solute in a fluid flowing through a tube. Proc Roy Soc London A 235: 67-77, 1956.

Bassingthwaighte, J.B., and Ackerman, F.H. Mathematical linearity of circulatory transport. J Appl Physiol 22: 879-888, 1967.

Bassingthwaighte, J.B., Malone, M.A., Moffet, T.C., King, R.B., Little, S.E., Link, J.M., and Krohn, K.A. Validity of microsphere depositions for regional myocardial flow. Am J Physiol 253: H184-H193, 1987.

Bergmann, S.R., Fox, K.A.A., Geltman, E.M., and Sobel, B.E. Positron transmission tomography of the heart. Prog Card Dis 28: 165-194, 1985.

Bergmann, S.R., Herraro, P., Weinheimer, C.J., and Walsh, M.N. (abstract presentation) Quantitative assessment of myocardial blood flow with oxygen-15 labeled water and positron emission tomography. Circ 78: II-599, 1988.

Bertin, E.P. Principles and Practice of X-ray Spectrometric Analysis. Plenum Press, New York, 1975.

Bettmann, M.A., and Morris, T.W. Recent advances in contrast agents. Rad Cl N Am 24: 347-357, 1986.

Boyd, D.P., Gould, R.G., Quinn, J.R., Sparks, R., Stanley, J.H., and Herrmansfeldt, W.B. A proposed dynamic cardiac 3-D densitometer for early detection and evaluation of heart disease. IEEE Trans Nucl Sci NS-26: 2724-2727, 1979.

Brasch, R.C., Boyd, D.P, and Gooding, C.A. Computed tomographic scanning in children: Comparison of radiation dose and resolving power of commercial CT scanners. Am J Roentgenol 131:95-101, 1978.

Braunwald, E. Introductory remarks. in Protection of the Ischemic Myocardium, ed. E. Braunwald, AHA Monograph Number 48: 1-2, 1976.

Buckberg, G.D., Luck, J.C., Payne, B.D., Hoffman, J.I.E., Archie, J.P., and Fixler, D.E. Some sources of error in measuring regional blood flow with radioactive microspheres. J Appl Physiol 31: 598-604, 1971.

Carlsen, O., and Hedegaard, O. Evaluation of regional cerebral circulation based on absolute mean transit times in radionuclide cerebral angiography. Phys Med Biol 32: 1457-1467, 1987.

Coulam, C.M., Warner, H.R., Wood, E.H., and Bassingthwaighte, J.B. A transfer function analysis of coronary and renal circulation calculated from upstream and downstream indicator-dilution curves. Circ Res 19: 879-890, 1966.

CRC Press, Handbook of Spectroscopy, vol 1, ed. J.W Robinson, Cleveland, 1974.

Davenport, R. The derivation of the gamma-variate for tracer dilution curves. J Nucl Med 24: 945-948, 1983.

Doherty, P.W., Lipton, M.J., Berninger, W.H, Skioldebrand, C.G., Carlsson, E., and Redington, R.W. Detection and quantitation of myocardial infarction in-vivo using transmission computed tomography. Circ 63: 597-606, 1981.

Evans, R. L. Two comments on the estimation of blood flow and central volume from dye-dilution curves. J Appl Physiol 14: 457, 1959.

Farmer, D., Lipton, M.J., Higgins, C.B., Ringertz, H., Dean, P.B., Sievers, R., and Boyd, D.P. In-vivo assessment of left ventricular wall and chamber dynamics during transient myocardial ischemia using cine computed tomography. Am J Card 55: 560-565, 1985.

Freund, R.J., and Minton, P.D., Regression Methods. Marcel Dekker, Inc., New York, 1979.

Grönberg, T., Sjoberg, S., Torsten, A., Golman, K., and Mattsson, S. Noninvasive estimation of kidney function by X-ray fluorescence analysis. Inv Rad 18: 445-452, 1983.

Hackländer, T., Szabo, Z., Vosberg, H., and Feinendegen, L.E. The use of gamma functions in the calculation of organ perfusion functions for non-diffusible radioactive tracers. Phys Med Biol 33: 53-59, 1988.

Hamilton, W.F., Moore, J.W., Kinsman, J.M., and Spurling, R.G. Studies on the circulation. Am J Physiol 99: 534-551, 1932.

Harpen, M.D., and Lecklitner, M.L. Derivation of gamma-variate indicator dilution function from simple convective dispersion model of blood flow. Med Phys 11: 690-692, 1984.

Harris, T.R., and Newman, E.V. An analysis of mathematical models of circulatory indicator-dilution curves. J Appl Physiol 28: 840-849, 1970.

Hays, J.R., Clements, W.C., Jr., and Harris, T.R. The frequency domain evaluation of mathematical models for dynamic systems. Am Inst Ch Eng J 13: 374-378, 1967.

Heymann, M.A., Payne, B.D., Hoffman, J.I.E., and Rudolf, A.M. Blood flow measurements with radionuclide-labeled particles. Prog Card Dis 20: 55-79, 1977.

Higgins, C.B., Sovak, M., Schmidt, W., and Siemers, P.T. Differential accumulation of radiopaque contrast material in acute myocardial infarction. Am J Card 43: 47-51, 1979.

Higgins, C.B., Gerber, K.H., Mattrey, R.F., and Slutsky, R.A. Evaluation of the hemodynamic effects of intravenous administration of ionic and nonionic contrast materials. Radiology 142: 681-686, 1982.

Hoffer, P.B. Fluorescent thyroid scanning. Am J Roentgen 105: 321-344, 1969.

Hoffer, P.B., Bernstein, J., and Gottshalk, A. Fluorescent technique in thyroid imaging. Sem Nuc Med 1: 379-389, 1971.

Hogg, R.V., and Tanis, E.A. Probability and Statistical Inference. Macmillan Publishing Co., New York, 1983.

Hubbell, J.H. Photon cross sections, attenuation coefficients, and energy absorption coefficients from 10 keV to 100 GeV. US Dept's of Commerce, Nat Bur Stnds NSRDS-NBS 29, 1969.

Hubbell, J.H. Photon mass attenuation and energy absorption coefficient from 1 keV to 20 MeV. Int J Appl Rad Iso 33: 1269-1290, 1982.

Jaschke, W., Gould, R.G., Assimakopoulos, P.A., and Lipton, M.J.. Flow measurements with a high-speed computed tomography scanner. Med Phys 14: 238-243, 1987.

Kajiya, F., Tomonaga, G., Tsujioka, K., and Ogasawara, Y. Evaluation of local blood flow velocity in proximal and distal coronary arteries by laser doppler method. J Biomech Eng 107: 10-15, 1985.

Kaufman, L., Shames, D.M., Greenspan, R.H., Powell, M.R., and Perez-Mendez, V. Cardiac output determination by fluorescence excitation in the dog. Inv Rad 7: 365-368, 1972.

Kinsman, J. M., Moore, J. W., and Hamilton, W. F. Studies on the circulation: I. Injection method: Physical and mathematical considerations. Am J Physiol 89: 322-330. 1929.

Koehler, R.E., Kaufman, L., Brito, A., and Nelson, J.A. In-vivo measurement of hepatic iodine concentration using fluorescence excitation analysis. Inv Rad 11: 134-137, 1976.

Lenhoff, A.M., and Lightfoot, E.N. The effects of axial diffusion and permeability barriers on the transient response of tissue cylinders, II. Solution in time domain. J Theor Biol 106: 207-238, 1984.

Leonard, E.F., and Jorgensen, S.B. The analysis of convection and diffusion in capillary beds. Ann Rev Biophys Bioeng 3: 293-339, 1974.

Levesque, M.J., and Nerem, R.M. Coronary flow characteristics as revealed by endothelial cell patterns. in Mechanics of Coronary Circulation. ed's R.E. Mates, R.M. Nerem, and P.D. Stein, ASME, New York, 1983.

Lipton, M.J. Quantitation of cardiac function by Cine-CT. Rad Cl N Am 23: 613-626, 1985.

Maseri, A., Caldini, P., Permutt, S., and Zierler, K.L. Frequency function of transit times through dog pulmonary circulation. Circ Res 26: 527-543, 1970.

Marcus, M.L., Wilson, R.F., and White, C.W. Methods of measurement of myocardial blood flow in patients: a critical review. Circ 76: 245-253, 1987.

McInerney, J.J., Copenhaver, G.L., and Herr, M.D. In-vivo cardiac muscle perfusion: a new measurement method. IEEE Trans BME-34: 251-255, 1987.

McInerney, J.J. Personal Communication, 1989.

Meier, P., and Zierler, K.L. On the theory of the indicator-dilution method for measurement of blood flow and volume. J Appl Physiol 6: 731-744, 1954.

Mullani, N.A., and Gould, K.L. Functional cardiac imaging: positron emission tomography. Hospital Practice, Feb: 103-118, 1984.

Nakai, M. Computation of transport function using multiple regression analysis. Am J Physiol 240: H133-H144, 1981.

Newman, E. V., Merrell, M., Genecin, A., Monge, C., Milnor, W. R., and McKeever, W. P. The dye dilution method for describing the central circulation: an analysis of factors shaping the time-concentration curves. Circ 4: 735-746, 1951.

Oppenheim, A.V., and Schafer, R.W. Digital Signal Processing. Prentice-Hall, Englewood Cliffs, New Jersey, 1975.

Palmer, B.M., McInerney, J.J., Copenhaver, G.L., and Herr, M.D. Perfusion characteristics measured by X-ray fluorescence. Proc 13th Ann Northeast Bioe Conf, pp. 223-226, 1987.

Palmer, B.M., and McInerney, J.J. A model to aid in the calculation of regional myocardial perfusion. Proc IEEE Eng Med Biol Soc 10th Ann Conf, pp. 133-134, 1988.

Papoulis, A. Signal Analysis. McGraw Hill Book Company, New York, 1977.

Perl, W.P., and Chinard, F.P. A convection-diffusion model of indicator transport through an organ. Circ Res 22: 273-298, 1968.

Phelps, M.E., Grubb, R.L., and Ter-Pogossian, M.M., Correlation between $P_a[CO_2]$ and regional cerebral blood volume by X-ray fluorescence. J Appl Physiol 35: 274-280, 1973.

Rubio, R., and Berne, R.M. Regulation of coronary blood flow. Prog Card Dis 18: 105-122, 1975.

Rumberger, J.A., Feiring, A.J., Lipton, M.J., Higgins, C.B., Ell, S.R., and Marcus, M.L. Use of ultrafast computed tomography to quantitate regional myocardial perfusion: a preliminary report. J Am Coll Card 9: 59-69, 1987.

Russ, J.C. Fundamentals of Energy Dispersive X-ray Analysis. Butterworths, Boston, 1984.

Rutishauser, W., Bussmann, W., Noseda, G., Meier, W., and Wellauer, J. Blood flow measurements through single coronary arteries by Roentgendensitometry. Part I: A comparison of flow measured by a radiologic technique applicable in the intact organism and by electromagnetic flowmeter. Am J Roentgenol 109: 12-20, 1970.

Schlossmacher, E.J., Weinstein, H., Lochaya, S., and Shaffer, A.B. Perfect mixers in series model for fitting venoarterial indicator-dilution curves. J Appl Physiol 22: 327-332, 1967.

Silber, E.N. Heart Disease. MacMillan Publishing Co., New York, 1987.

Sjoberg, S., Torsten, A., Golman, K., Grönberg, T., and Mattsson, S. Noninvasive estimation of kidney function by X-ray fluorescence analysis: biological half-life and clearance of contrast material in rabbits. Inv Rad 16: 215-220, 1981.

Snyder, D.L. Random Point Processes. John Wiley & Sons, New York, 1975.

Spalding, D.B. A note on mean residence times in steady state flows of arbitrary complexity. Chem Eng Sci 9: 74-77, 1958.

Starmer, C.F. and Clark, D.O. Computer computations of cardiac output using the gamma-function. J Appl Physiol 28: 219-220, 1970.

Stewart, G.N. Output of the heart. J Physiol 22: 159-183, 1897.

Stewart, G.N. Pulmonary circulation time, the quantity of blood in the lungs and the output of the heart. Am J Physiol 58: 20-44, 1921.

Strauss, H.W., and Boucher, C.A. Myocardial perfusion studies: lessons from a decade of clinical use. Radiology 160: 577-584, 1986.

Tamaki, N., Mukia, I., Ishii, Y., Fujita, T., Yamamoto, K., Minato, K., Yonejura, Y., Tamaki, S., Kambara, H., Kawai, C., and Torizuka, K. Comparative study of thallium emission tomography with 180° and 360° data collection. J Nucl Med 23: 661-666, 1982.

Taylor, G. Dispersion of soluble matter in solvent flowing slowly through a tube. Proc Roy Soc London A 219: 186-203, 1953.

Taylor, G. Conditions under which dispersion of a solute in a stream of solvent can be used to measure molecular diffusion. Proc Roy Soc London A 225: 473-477, 1954.

Tepper, R.S., Lee, H.L., and Lightfoot, E.N. Transient convective mass transfer in Krogh tissue cylinders. Ann Biomed Eng 6: 506-530, 1978.

Ter-Pogossian, M.M., Phelps, M.E., and Lassen, M. In-vivo measurement of regional cerebral blood flow and blood volume by means of stimulated X-ray fluorescence, Part A-Methodology. in Semiconductor Detectors in Nuclear Medicine. ed.'s P.B. Hoffer, R.N. Beck and A. Gottshalk, pp. 240-257, Society of Nuclear Medicine, New York, 1971.

Thompson, H. K., Jr., Starmer, C., Whalen, R. E., and McIntosh, H.D. Indicator transit time considered as a gamma-variate. Circ Res 10: 502-515, 1964.

Vaño, E., and González, L. Importance of geometry in biological sample analysis by X-ray fluorescence. Med Phys 5: 400-403, 1978.

Whiting, J.S., Drury, J.K., Pfaff, J.M., Chang, B.L., Eigler, N.L., Meerbaum, S., Corday, E., Nivatpumin, T., Forrester, J.S., and Swan, H.J.C. Digital angiographic measurement of radiographic contrast material kinetics for estimation of myocardial perfusion. Circ 73: 789-798, 1986.

Wolfkiel, C.J., Ferguson, J.L., Chomka, E.V., Law. W.R., Labin, I.N., Tenzer, M.L., Booker, M., and Bundage, B.H. Measurement of myocardial blood flow by ultrafast computed tomography. Circ 76: 1262-1273, 1987.

Wolpers, H.G., Geppert, V., Hoeft, A., Korb, H., Shrader, R., and Hellige, G. Estimation of myocardial blood flow heterogeneity by transorgan helium transport functions. Pflügers Archiv 401: 217-222, 1984.

Yoder, R.D. and Swan, E.A. Cardiac output: Comparison of Stewart-Hamilton and gamma-function techniques. J Appl Physiol 31: 318-321, 1971.